UCRL--21085

DE88 016174

THEORETICAL STUDY OF TURBULENT CHANNEL FLOW: BULK PROPERTIES, PRESSURE FLUCTUATIONS, AND PROPAGATION OF ELECTROMAGNETIC WAVES

V. M. Canuto, G. J. Hartke, A. Battaglia, J. Chasnov

NASA Goddard Space Flight Center

Institute for Space Studies

2880 Broadway

New York, NY 10025

and

G. F. Albrecht

Mail Code L

Lawrence Livermore National Laboratory

Livermore, Ca. 94550

ABSTRACT

In this paper, we apply two theoretical turbulence models, DIA and the recent GISS model, to study properties of a turbulent channel flow. Both models provide a turbulent kinetic energy spectral function E(k) as the solution of a non–linear equation: the two models employ the same source function but different closures. The source function is characterized by a rate $n_s(k)$ which is derived from the complex eigenvalues of the Orr–Sommerfeld (OS) equation in which the basic flow is taken to be of a Poiseuille type. The O–S equation is solved for a variety of Reynolds numbers corresponding to available experimental data. A physical argument is presented whereby the central line velocity characterizing the basic flow, U_0^L, is not to be identified with the U_0 appearing in the experimental Reynolds number. A renormalization is suggested which has the effect of yielding growth rates of magnitude comparable to those calculated by Orszag and Patera based on their study of a secondary instability. From the practical point of view, this renormalization frees us from having to solve the rather time consuming equations describing the secondary instability. This point is discussed further in XII. In the present treatment, the shear plays only the role of a source of energy to feed the turbulence and not the possible additional role of an interaction between the shear of the mean flow and the eddy vorticity that would give rise to resonance effects when the shear is equal to or larger than the eddy vorticities. The inclusion of this possible resonance phenomenon, which is not expected to affect the large eddy behavior and thus the bulk properties, is left for a future study. The theoretical results are compared with two types of experimental data: a) turbulence bulk properties, Table IV and b) properties that depend strongly on the structure of the turbulence spectrum at low wave numbers (i.e., large eddies), Tables V and VI. The latter data are taken from recent experiments measuring the changes in the propagation of an electromagnetic wave through a turbulent channel flow. The fluctuations in the refractive index of the turbulent medium are thought to be due to

pressure fluctuations whose spectral function $\Pi(\mathbf{k})$ is contributed mostly by the interaction between the mean flow and the turbulent velocity. The spectrum $\Pi(\mathbf{k})$ must be computed as a function of the wave number $\mathbf{k}$, the position in the channel x_2, and the width of the channel Δ. The only existing analytical expression for $\Pi(\mathbf{k})$, due to Kraichnan, cannot be used in the present case because it applies to the case $x_2=0$ and $\Delta=\infty$, which corresponds to the case of a flat plate, not a finite channel. A general expression for $\Pi(\mathbf{k},x_2,\Delta)$ is derived here for the first time and employed to calculate the fraction of incoherent radiation scattered out of a coherent beam. In Section XI, we treat anisotropy and show how to extend the previous results to include an arbitrary degree of anisotropy in the sizes of the eddies. We show that the theoretical one–dimensional spectra yield a better fit to the data for a degree of anisotropy ($\alpha \approx 4$) that is within the range of experimental values. We also extend the expression for $\Pi(\mathbf{k},x_2;\Delta)$ to $\Pi(\mathbf{k},x_2;\Delta,\alpha)$ and compute the pressure fluctuations for different values of α. Similarly, we evaluate the fraction of electromagnetic energy scattered by an anisotropic turbulent flow and find a good fit to the laboratory data for a value of $\alpha \approx 4-6$.

Theoretical problems however remain which will require further study: among them, lack of backscatter (i.e., the transfer of energy from large to small wavenumbers) in the GISS model, possible resonance effects between the shear and eddy vorticity, behavior of the one dimensional spectral function at low wavenumbers, and the role of the secondary instability. These topics are now under investigation.

I. INTRODUCTION

Experimental data on turbulent channel flow[1–6] can be used to test the validity of theoretical descriptions of turbulence. The latter can be broadly divided into two categories: numerical simulation of the Navier–Stokes equations and theoretical closure models.

While direct numerical simulations[7,8] have successfully reproduced several experimental data, they are limited to low Reynolds numbers since the number of grid points required increases according to the 9/4 power of the Reynolds number and the number of time steps needed for an accurate simulation increases according to the 3/4 power, yielding a rate of increase of Reynolds number to the third power. For high Reynolds number flows, the required number of grid points rapidly outstrips presently available computational facilities. To treat high Reynolds number turbulent flows, large eddy simulations make use of (empirical) subgrid scale models.[8]

Theoretical closure models can be broadly divided into two categories: single–point and two–point closure models. The most well–known among the former is the one originally proposed by Hanjalic and Launder (HL),[9] which proved successful in describing several types of shear flows. The HL model provides three coupled differential equations for the Reynolds stress tensor τ_{12}, the energy dissipation rate ϵ, and the turbulent kinetic energy K, defined as the integral over all wavenumbers k of the turbulent energy spectral function E(k). The latter is known to satisfy the following equation[10–12] (Ref. 9, Eq. 4.4; Ref. 10, Eqs. 4.35 or 4.38; Ref. 12, Eq. 15.27),

$$\frac{\partial}{\partial t}\int_0^k E(k)\,dk + s\int_0^k E_{12}(k)\,dk + 2\nu\int_0^k k^2 E(k)\,dk = -\int_k^\infty T(k)\,dk\,, \qquad (1)$$

where s is the shear, E_{12} is the spectral energy function of the Reynolds stress tensor, and T(k) is the non–linear transfer among eddies of different wavenumbers. Eq. (1) can easily be rewritten to exhibit the energy dissipation rate, ϵ, by extending the k integration to infinity and then subtracting the result from (1).

The HL model proposes an equation for this quantity which must be solved simultaneously with (1) and with the equation for ϵ. As previously stated, the HL model has proven very successful in the detailed description of several types of shear flows, its main drawback being the presence of six parameters that the model cannot determine.

The HL model had actually been preceded by the work of Tchen[11] who suggested a physically interesting model based on the possibility of resonance interactions when the eddy vorticity is equal to or greater than the shear of the mean flow. The need for an equation for E_{12} was bypassed, for the model suggested an expression for it in terms of E(k) and T(k) themselves. Although the model introduces two free parameters, it proved successful in predicting not only the existence of an inertial Kolomogoroff region but also the existence of a k^{-1} range that was actually verified experimentally. Tchen's model is physically attractive and it would be interesting to try and improve on it.

In the early seventies, Leslie[12] was the first to consider in detail the possible application of two–point closure models to turbulent channel flow. Upon realizing the unmanageable complexity of the DIA equations for the general case of shear flow,[13] Leslie tried to develop a systematic program of simplifications for the two–point closure equations by restricting the analysis to the case of anisotropic but homogeneous flow (i.e., with constant shear) in the hope of deriving in a deductive, parameter free fashion, the empirical one–point closure relations of Hanjalic and Launder.[9] By his own surmising, Leslie did not

succeed in his attempt.

Since Leslie's work was not followed by other attempts to employ two–point closure models to turbulent channel flow, one is left today with either the successful one–point HL closure model which, however, contains six free parameters to be determined from experiments, with direct numerical simulations with their intrinsic Reynolds number limitations, or with a large eddy simulation which must rely on the use of a subgrid scale model.

The model we are about to present contains no free parameters, employs (two) closure models and, within the goals it sets for itself, can be said to be relatively successful. The models used in this paper contain features that are common to the HL model, to Leslie's attempt, and to Tchen's physical approach. In common with the latter is the fact that our work deals with only one equation, the one for the turbulent kinetic energy spectral function E(k), but at the same time it differs from Tchen's work in that $E_{12}(k)$ is not written phenomenologically in terms of E(k) and T(k). Rather, it is considered in the same spirit of the HL work, namely derived from an external relation, see IV. Our model has in common with Leslie's approach the treatment of the non–linear transfer terms, but it overcomes the difficulty that he had in treating anisotropy (caused by the mean flow stretching the eddies in the streamwise direction) by adopting a less formal but physically appealing approach originally proposed by Kraichnan.[28,29] We first derive expressions for all of the quantities of interest, i.e., the one–dimensional energy spectrum, the amplitude of the pressure fluctuations, and the attenuation of a laser beam in the stretched physical system where the wavenumbers are denoted by $\mathbf{k}'$. These functions depend on $E(k')$, the turbulent energy spectral function in the anisotropic system. However, since present turbulence models only allow us to calculate the energy spectrum, E(k), in isotropic systems, we have introduced an aspect ratio or anisotropy parameter, α, a measure of the

stretching of the eddies in the streamwise direction, such that $k_1' = k_1/\alpha$, $k_2' = k_2$, and $k_3' = k_3$. By transforming from the $\mathbf{k}'$ to the $\mathbf{k}$ system, we then perform the integrations in $\mathbf{k}$ space. The final expressions will depend on the anisotropy parameter α which is not known *a priori* but must be determined through comparison with experimental data. By comparing predicted and experimental one–dimensional spectra, we found that the best fit was for $4 \leq \alpha \leq 8$. The amplitude of the pressure fluctuations at the walls is most sensitive to the value of α (since the flow tends toward isotropy at midchannel) and a value of α in the range 4 to 6 was found to best fit the measured values. In the calculation of the attenuation of a laser beam propagating through a channel flow, we again found a best fit to the data for α in the range of 4 to 6. The consistency of these results lends credence to the methodology employed.

As stated earlier, we shall adopt the DIA as well as the recent GISS model.[14] The latter has been recently tested against several types of turbulence, convection, grid turbulence, shear, etc. In all cases considered, the results were satisfactory.

Notation: while in the DIA model the spectral energy function is denoted by E(k), in the GISS model use is made of the function $F(k) = 2E(k)$.

II. THE GISS MODEL

The GISS model is based on a physical representation of the non–linear energy transfer in a way that while reminiscent of the work of Heisenberg,[15] generalizes it in two important aspects, as described below. Assuming the turbulence is stationary, we begin by writing Eq. (1) as

$$\epsilon(k) = 2\nu\int_0^k k^2 E(k)\, dk + \int_k^\infty T(k)\, dk\,, \tag{2}$$

where

$$\epsilon(k) = 2\int_0^k \left[n_s(k) + \nu k^2\right] E(k)\, dk \tag{3}$$

is the rate of energy input into the wavenumber interval [0,k], which is partly dissipated by molecular viscosity and partly transferred by the non–linear term, T(k). The DIA and GISS models differ in the way they describe the function T(k).

Equation (2) separates the action of the source, represented by $\epsilon(k)$, from the action of viscosity and the non–linearity. Clearly, the separation is not meant to imply that $\epsilon(k)$ does not depend on the same ingredients that enter into the right hand side of the equation. it only helps in visualizing the physics of Eq. (1) more clearly. The problem then reduces to the evaluation of the quantity $n_s(k)$, the rate at which energy is being fed into the system. A discussion of how to compute this quantity will be given in Section IV. For the time being, we shall only note that the structure of $n_s(k)$ must be such that it depends on the source of energy for the turbulent flow, namely the shear itself. That this is indeed the case, will be shown in Eqs. (53)–(54).

We begin by writing the transfer term T(k) as the product of a turbulent viscosity times a mean square vorticity, i.e.,

$$\int_k^\infty T(k)\, dk = \nu_t(k) y(k)\,, \qquad y(k) = \int_0^k k^2\, F(k)\, dk\,, \tag{4}$$

so that the equation describing the energy balance in a turbulent flow becomes

$$\epsilon(k) = [\nu + \nu_t(k)]\, y(k). \tag{5}$$

If one adopts the expressions

$$\nu_t(k) = \int_k^\infty \left[\frac{F(k)}{k^3}\right]^{\frac{1}{2}} dk\,, \qquad \epsilon(k) = \epsilon = \text{constant}\,, \tag{6}$$

Eq. (5) reduces to the well known Heisenberg model that successfully reproduces the inertial subrange form of $F(k) \propto k^{-5/3}$, when ν_t is greater than ν.

The GISS model adopts the form of Eqs. (4) and (5) but neither of Eqs. (6). It extends both expressions in such a way that they reduce to (6) **only** in the inertial subrange. The generalization is carried out in two steps. First, the expression for $\epsilon(k)$, rather than being taken to be a constant independent of k, is written as

$$\epsilon(k) = \int_0^k F(k)\,(n_s(k) + \nu k^2)\, dk\,, \tag{7}$$

where νk^2 cancels the negative viscosity effects included in $n_s(k)$: the latter represents the rate at which energy is pumped into the system in the wavenumber interval between 0 and k. It is expected that for sufficiently large k, the integrand vanishes since $n_s \to -\nu k^2$. Thereafter, $\epsilon(k)$ remains constant. Then the Heisenberg approximation, $\epsilon(k) = \text{constant} = \epsilon$ is valid.

The second generalization consists of writing the turbulent viscosity as

$$\nu_t(k) = \int_k^\infty \frac{F(k)}{n_c(k)}\, dk \,, \tag{8}$$

where $n_c(k)$ is a correlation time between eddies, to be determined by a closure. Equations (7) and (8) represent a formal generalization of the Heisenberg expressions. The essence of the GISS model is contained in a new closure, i.e. an expression relating $n_c(k)$ to $F(k)$ and $n_s(k)$, the latter being considered given, either from an independent calculation (see Section IV) or self–consistently.[14]

Differentiating Eq. (5) with respect to k and making use of Eqs. (7) and (8), one obtains

$$n_s(k) + \frac{y(k)}{n_c(k)} = k^2 \nu_t(k) \,. \tag{9}$$

The GISS model closure is represented by

$$k^2 \nu_t(k) = \gamma\, n_c(k) \,, \tag{10}$$

which, when inserted into Eq. (9), yields an expression for $n_c(k)$ in terms of $n_s(k)$ and $y(k)$, namely,

$$2\gamma n_c(k) = n_s(k) + [n_s^2(k) + 4\gamma y(k)]^{\frac{1}{2}} \,. \tag{11}$$

Substituting (11) into (9) and using (8), one obtains a non–linear differential equation for

F(k). This is equivalent to solving a non–linear equation for the auxiliary function V(k) defined as $V(k) = y(k) + \gamma n_c^2(k)/2$, i.e.,

$$\frac{dV(k)}{dk} = \frac{2\gamma n_c^2(k)}{k} \tag{12a}$$

$$3\gamma n_c(k) = n_s(k) + [n_s^2(k) + 6\gamma V(k)]^{\frac{1}{2}} . \tag{12b}$$

Since $dy(k)/dk = k^2F(k)$, the knowledge of V(k) yields the spectral function, F(k). The paramete, γ is the only free parameter in the model and was found to be related to the Kolmogoroff constant Ko by the expression

$$\gamma = \left[\frac{2}{3Ko}\right]^3. \tag{13}$$

One can easily show that the Heisenberg model is indeed contained in the GISS model. For eddies sufficiently removed (in k space) from the source, which acts primarily at low wavenumbers, the time scale characterizing the source, n_s^{-1}, is no longer the dominant one. The eddy dynamics are governed primarily by the local break–up mechanism characterized by a time scale given by the vorticity, so that when $y^{\frac{1}{2}} >> n_s$, $n_c \propto y^{\frac{1}{2}}$, and Eq. (8) reduces to the Heisenberg form given by Eq. (6), at least for a power law F(k). At the same time, far from the source, the function $\epsilon(k)$ saturates, i.e., $\epsilon(k) = \epsilon =$ constant, Eq. (6). This shows that the GISS model encompasses the inertial subrange. On the other hand, for eddies with sizes of the order of the dimensions of the system itself, one may expect that the dominant time scale would be closer to that of the source, i.e. $n_s >> y^{\frac{1}{2}}$, $n_c \sim n_s$, and clearly $\epsilon(k)$ is not constant. Under these conditions, one cannot expect a universal form for the energy spectral function, since F(k) now depends on the specific form of the stirring mechanism.

In conclusion, while the Heisenberg model yields a universal F(k), the GISS model yields an F(k) which is a universal function of $n_s(k)$.

III. THE DIA MODEL

Perhaps the most well known of the presently available theories to describe fully developed turbulence is Kraichnan's direct interaction approximation[16] (DIA) which in turn has given rise to other theories which bear the same spirit. We shall not discuss here the eddy damped quasi–normal Markovian (EDQNM) approximation, which is phenomenological in nature, since the eddy correlation time scale (which within the DIA is determined by solving the integral equation satisfied by the infinitesimal response function) must be chosen using external inputs. A very complete description of EDQNM, its successes and limitations in describing "universal" properties can be found in Ref. 17.

Since the DIA has been described in detail elsewhere,[12] we shall present only the basic equations for the turbulent energy spectral function. Although the DIA is a well understood approximation to the non–linear transfer terms,[18] it can be regarded as a fully deterministic theory without free parameters. Since the DIA formalism has in the past been applied primarily to describe those properties of turbulence that do not depend on the specific nature of the source function, experimental data concerning bulk properties could not be dealt with. To include them, the DIA was recently applied with good results to a set of model equations with a source function appropriate to high Rayleigh number convection.[19] Perhaps the main drawback in the application of the DIA formalism to specific cases of interest has been the rather intimidating nature of the equations describing the turbulent energy spectral function, E(k). Moreover, with the presence of the infinitesimal response function G(k), one must in fact solve two coupled integral equations

for E(k) and G(k). These equations may be written[19]

$$\left[\frac{\partial}{\partial t} - n_s(k)\right] Q(k,t-s) = 2\pi \iint^{\Delta} kqp\, b(k,q,p)\, dq\, dp$$

$$\times \left[\int_{-\infty}^{s} ds'\, G(k,s-s')Q(q,t-s')Q(p,t-s') \right.$$

$$\left. - \int_{-\infty}^{t} ds'\, G(q,t-s')Q(p,t-s')Q(k,s-s') \right] \qquad (14)$$

and

$$\left[\frac{\partial}{\partial t} - n_s(k)\right] G(k,t-s) = -2\pi \iint^{\Delta} kqp\, b(k,q,p)\, dq\, dp \int_{s}^{t} ds'\, G(q,t-s')Q(p,t-s')G(k,s-s')$$

$$+ \delta(t-s), \qquad (15)$$

where $Q(k,t-s) = \langle u_i(\mathbf{k},t)u_i(-\mathbf{k},s) \rangle$, $\mathbf{u}(\mathbf{k},t)$ is the Fourier component of the turbulent velocity, the angular brackets denote a realization average, t and s are time variables, the energy spectrum is given by $E(k)=4\pi k^2 Q(k,0)$, $b(k,q,p) = (q/k)(xy+z^3)$ with x, y, and z the cosines of the angles opposite **k**, **q**, and **p**, respectively, $\delta(x)$ is the Dirac delta function, and the Δ over the wavenumber integrals indicates that the region of integration is restricted to a subdomain in which **k**, **q**, and **p** form a triangle. Once the growth rate $n_s(k)$ is specified, Eqs. (14) and (15) can be solved for the energy spectrum and the infinitesimal response function.

IV. THE RATE $n_s(k)$

Neither the DIA nor the GISS model can be expected to fix the functional form of $n_s(k)$ which must be provided by considerations other than the ones that led to the equations for the kinetic energy spectral function F(k). Prescribing an $n_s(k)$ is physically equivalent to prescribing an equation or a formula for the energy rate $\epsilon(k)$ since

$$\epsilon(k)=2\int_0^k (n_s(k)+\nu k^2)\, E(k)\, dk\,, \tag{2}$$

$$\epsilon = \epsilon(\infty) = 2\int_0^\infty (n_s(k)+\nu k^2)\, E(k)\, dk = 2\nu\int_0^\infty k^2 E(k)\, dk\,.$$

Our model can thus be considered a two equation model, one for the kinetic energy K,

$$K = \int_0^\infty E(k)\, dk\,, \tag{16}$$

and the second equation for $\epsilon(k)$. For a successful application of our model, the identification of the physically correct function $n_s(k)$ is clearly of critical importance. To that end, let us first discuss its physical meaning. From Eq. (9), we derive that

$$n_s(k) = k^2\nu_t(k) - n_d(k)$$

$$n_d(k) = \frac{1}{n_c(k)}\int_0^k k^2 E(k)\, dk\,, \tag{9}$$

i.e., the rate n_s is the difference between two rates: the rate $k^2\nu_t(k)$ at which energy, under the action of the non–linear interactions, cascades to all wavenumbers larger than the one considered (in fact, $\nu_t(k)$ is an integral from k to infinity), minus the rate at which energy is injected at k from all wavenumbers less than the one considered (since the the vorticity y(k) is an integral from 0 to k).

Since n_s represents a difference of rates characterizing the fully developed turbulent flow, i.e., long after the transition from the laminar state has occurred, it cannot *a priori* be identified with the instability function n_s^{L-T} that characterized the transition between laminarity (L) and turbulence (T), even though the processes they represent are physically equivalent. To derive n_s^{L-T}, one has a well defined mathematical formalism, the stability theory. To derive $n_s(k)$ or, equivalently, $\epsilon(k)$, one would have to construct another equation thus making the model much more complex. We have already shown[14] that physical arguments can be very helpful. Some general considerations are in order. First, it is known experimentally that, for example, in thermal convection the large scale structures that one observes at the transition do persist in the turbulent phase, i.e., their structure survives the strongly diffusive and shearing action of a turbulent flow. This result is perhaps not unexpected since the large scale structures have the longest lifetimes of all the eddies and also because their structure is affected primarily by the source rather than by the non–linear transfer interactions. Stated differently, since the largest eddies cannot originate from even larger ones, their sole source of growth is the source itself. Second, from a mathematical point of view it would clearly be greatly advantageous if one could employ, even if partially, the well established mathematical framework of stability theory to gain information about the form of the function $n_s(k)$. Here we want to make a clear distinction between the shape of the function $n_s(k)$ and its amplitude. We shall propose, and try to justify, that the former can be arrived at by the use of the Orr–Sommerfeld equation, while the latter can be arrived at only by providing a way to account for the

presence of a turbulent flow. The latter is in fact likely to renormalize in a significant way the amplitudes of the parameters characterizing the laminar regime. This in turn translates into a renormalization of the O–S equation itself. The success of the calculations presented in this paper will be seen to depend to a large extent on the proper implementation of this renormalization procedure. Since the latter depends on the specific problem at hand, it cannot be formulated in a universal fashion. Each physical problem brings in its own characteristic features. From the point of view of trying to understand a complex phenomenon like turbulence, we consider this to be an advantage, for the method requires an understanding of the renormalization that the most prominent features of the laminar flow have undergone. The use of an O–S type of equation to determine the functional form of the rate n_s is proposed here because such a function has features of almost universal character that are bound to be sufficiently well described by such an approach. First, consider the shape of $n_s(k)$. For wavenumbers less than $k_0 = 1/L$, where L is the geometrical dimension of the system under consideration, there cannot be any forcing and so n_s must be less than or equal to zero. On the other hand, for large values of k, i.e., when one deals with small eddies, the dominant mechanism is kinematic viscosity which contributes a factor $-\nu k^2$, i.e., the function n_s must become negative at some large value of k. In Ref. 14 it was shown that the GISS model requires that for large k, $n_s \sim -\nu k^2$ quite independently of its behavior at low wavenumber, i.e., of the specific mechanism that feeds energy into the turbulent regime. One may therefore conclude that the general shape of this function must be of the form shown in Fig. (1). In our experience with different types of turbulence, i.e., grid turbulence, thermal convection, and shear, we have indeed verified that the physical $n_s(k)$ has the form of Fig. (1). For example, in the case of grid turbulence where both the kinetic energy spectral function E(k) and the non–linear transfer term T(k) have been measured experimentally, one can derive $n_s(k)$ directly from the data since from Eqs. (2) and (3) it follows that

$$2n_s(k) = -\frac{T(k)}{E(k)} . \qquad (17)$$

The functions E(k) and T(k) are presented in Figs. (14) and (16) of Ref. 14. As one can see, the ratio does indeed have the shape of Fig. (1).

A second, parallel argument as to the validity of an O–S type equation as a guide to the functional form of n_s can be seen by using a procedure first suggested by Synge[20] whereby the O–S equation[20–23] is formally rewritten so as to exhibit the instability function or growth rate n_s (we shall omit the superscripts L–T). The result is (see Eq. 53 below)

$$n_s(k) = A\tau_{12}(k) - \nu B(k) , \qquad (18)$$

which shows, as expected on physical grounds, that n_s is composed of two terms: a source term, proportional to the shear τ_{12}, and a sink proportional to the viscosity ν. The O–S equation further predicts that the shear peaks near the walls (see Fig. 4.21 of Ref. 23), thus implying that in that region energy is extracted from the mean flow and fed into turbulence. Experimentally, it is known (see Fig. 5.5 of Ref. 24) that the main source of energy production, i.e., of $\epsilon(k)$, occurs precisely in that region. Thus, the O–S equation predicts correctly the physically important feature of a region of instability. There, the main physical process is intrinsically the same as the one that characterized the transition from laminarity to turbulence. That feature has thus survived even in the presence of turbulence, which one may hope can be accounted for by a process of renormalization for which we shall propose two methods and show that they yield very similar results.

We choose a coordinate system in which the mean flow is in the x–direction with one wall of the channel at y = –D and the other at y = D. Consider the well–known laminar Poiseuille profile,[24] with $\mathcal{y}$= y/D,

$$U(y) = \frac{D^2}{2\nu}\left[\frac{\Delta p}{\ell}\right](1-\mathcal{y}^2)\,. \tag{19}$$

where $\Delta p/\ell$ is the pressure drop along the channel of width 2D (we have taken unit density). In terms of the bulk velocity U_m defined as the integral across the channel of U(y) divided by the width of the channel, 2D, i.e.,

$$U_m = \frac{D^2}{3\nu}\frac{\Delta p}{\ell}\,, \qquad R_m = \frac{U_m D}{\nu}\,, \tag{20}$$

Eq. (19) becomes, where L stands for linear,

$$U(y) = U_0^L\,(1-\mathcal{y}^2)\,, \qquad U_0^L = \frac{3}{2}\,U_m\,, \tag{21}$$

and U_0^L is the value of U(y) at midchannel, $\mathcal{y}=0$.

As one can see, in the linear regime the pressure drop is proportional to U_m. This is no longer valid in the turbulent regime, where the relation is quadratic rather than linear. We shall propose to incorporate this physical property into (19) as a way to renormalize for the presence of turbulence. In order to do so, it is convenient to introduce the friction coefficient λ defined as[25]

$$\lambda = \frac{\tau_0}{\frac{1}{8}\,U_m^2}\,, \qquad \tau_0 \equiv D\,\frac{\Delta p}{\ell}\,, \tag{22}$$

so that Eq. (19) becomes

$$U(y) = \frac{\lambda D}{16\nu} U_m^2 (1 - \mathscr{y}^2) . \tag{23}$$

While this new form does not introduce any new physics at the laminar level, being merely a rewriting in terms of different variables, it does allow us to incorporate turbulence effects if an additional relation for the quantity λ is introduced, for example the one proposed by Blasius,[25] i.e.,

$$3\lambda = R_m^{-1/4} . \tag{24}$$

Eq. (23) can then be written as

$$U(y) = U_0^R (1 - \mathscr{y}^2) , \qquad U_0^R = \frac{\nu}{16D} \lambda R_m^2 , \tag{25}$$

where U_0^R is the renormalized midchannel velocity. Had we assumed that Eq. (21) were valid in the turbulent regime, we would have

$$U_0^L = \frac{3\nu}{2D} R_m , \tag{26}$$

which shows that the renormalization procedure from Eq. (21) to Eq. (25) is equivalent to taking

$$U_0^L \rightarrow U_0^R = \frac{\lambda}{24} R_m U_0^L . \tag{27}$$

It remains to relate R_m to the experimental R_{exp},

$$R_{exp} = \frac{U_0 D}{\nu} , \tag{28}$$

where U_0 is the measured center line (i.e., midchannel) velocity. The relationship between R_{in} and R_{exp} is given by[4,25]

$$R_{exp} - R_m = 2.53\, R_\tau\,, \qquad R_\tau = \frac{\tau_0^{\frac{1}{2}} D}{\nu}\,, \tag{29}$$

where the ratio R_{exp}/R_τ can be expressed alternatively as [3,4,25] (κ=0.41, B=5.1)

$$\frac{1}{\kappa} \ln R_\tau + B, \qquad 9.268\, R_{exp}^{0.089}, \qquad 25 + 3.5 \times 10^{-3}\, R_\tau\,. \tag{30}$$

A second approach for renormalizing the laminar profile can be devised by considering that the experimentally measured mean velocity field, U(y), does indeed retain some vestiges of the laminar profile in the region near the walls where the energy is being produced. This can be seen by recalling the experimental form of U(y) as given for example in Ref. 25, i.e.,

$$U(y) = U_\tau\, R_\tau\, (1-|y|) \qquad R_\tau(1-|y|) \le 10 \tag{31a}$$

$$U(y) = U_\tau \left[\frac{5}{2} \ln R_\tau\, (1-|y|) + 5.1\right] \qquad R_\tau(1-|y|) > 10\,, \tag{31b}$$

and Fig. (5.5) of Ref. 24 which shows that the maximum production occurs at the point where the linear regime changes to the logarithmic one. To renormalize the profile (19), we must eliminate the pressure gradient in terms of some other physical characteristic of the turbulent regime. We shall proceed as follows. Since both the profile (19) and the experimental one given by (31) are linear in the region where energy is being produced most efficiently, we shall require that the slope of the two functions be the same as y goes to −D so as to assure that the two are identical in that region. This implies that $\Delta p/\ell = U_\tau^2/D$, which in turn implies that

$$U(y) = U_0^R (1 - y^2) , \qquad U_0^R = \frac{\nu}{2D} R_\tau^2 . \tag{32}$$

In this case we note that the renormalization for U_0^L is given by

$$U_0^L \rightarrow U_0^R = \frac{\nu}{3D} \frac{R_\tau^2}{R_m} U_0^L . \tag{33}$$

In Table I, we present some numerical results that show how the two renormalizations, Eq. (27) and (33) yield similar results ($r_1 = R_m^{3/4}/72$, $r_2 = R_\tau^2/3R_m$). Considering the empirical nature of some of the relations employed in the previous derivation, the agreement of the results calculated using the two methods may be considered quite good.

It is probably not a coincidence that for $R_{exp}=10^4$, we get a renormalization factor that is very close to the one first obtained by Reynolds and Tiederman[26] more than twenty years ago and recently reconfirmed.[27] Both studies point out that the use of the experimental form of $U_{exp}(y,R_{exp})$ in the O–S equation yields stable solutions, i.e., $n_s<0$, *if* it is assumed that the Reynolds number appearing explicitly in the O–S equation, R_{O-S}, which is in effect a viscosity, is to be the same as the R_{exp} entering $U_{exp}(y,R_{exp})$. On the other hand, if R_{O-S} is left as a free parameter, unstable solutions ($n_s>0$) can be obtained if

$$R_{O-S} \sim (10 - 15) R_{exp} . \tag{34}$$

It is as if the effect of turbulence is equivalent to a decrease of the molecular viscosity. At first this may sound incorrect for we know that when dealing with the mean flow equations, the molecular viscosity is increased by the effect of turbulence and, by extrapolation, one

might expect that the same would be true when considering not the equation for the mean flow but for the turbulent flow itself. The only phenomenon that comes to mind that could play the role of an internal source of energy, thus a lowering of the viscosity, is backscatter, a mechanism whereby the energy in the high wavenumber regions does not cascade to still higher wavenumbers (in the direction of the increasing importance of viscosity) but is scattered back to lower wavenumbers, thus in effect playing against viscosity.

In conclusion, the rate n_s entering in (3) is not the rate that characterizes the transition from laminarity to turbulence. Rather, it represents the rate at which energy is pumped into turbulence in such a way as to satisfy (9), which represents the balance between the rate at which such an energy is put into the system and the non–linear terms, $k^2\nu_t$, that either transfer it to higher wavenumbers or feed the same wavenumber interval with energy from lower wavenumbers, $y(k)n_c^{-1}(k)$. The quantity n_s represents an instability, but one in the presence of turbulence. In the case of channel flow, a region can be isolated near the walls where there is such an instability in the sense that the energy is being extracted from the mean flow and given to the turbulence. In that region, the velocity profile is linear. We have tried to extract information about the rate at which such energy is transferred from one type of flow to the other by using the O–S equation in which, however, the strength of the mean flow was adjusted to match the experimental one. In that sense, the O–S equation must be viewed more as a phenomenological tool rather than the exact equation that it really is when one deals with the very different problem of the transition between laminarity and turbulence.

There are, however, two other ways of looking at the rate n_s. One could renounce any attempt at deriving n_s from a mathematical equation, but rather consider it as a phenomenological function of the type

$$n_s = n_s(k,a,b) \,, \tag{35}$$

where the analytical form can be taken to match Fig. 1, and where the parameters a and b can be fixed by demanding that the total kinetic energy K and the rate ϵ derived from the turbulence model match the experimental values. By adopting this procedure, one transforms the model into one that, rather than predicting the turbulent quantities becomes a tool to assess the correctness of the non–linear transfer terms, i.e., the validity of the adopted closure model. This method was successfully adopted in Ref. 14 in the case of grid turbulence, where the predicted transfer term T(k) was found to compare rather well with the measured value. (See Fig. 16 of Ref. 14.)

Another possible way of using the present model of turbulence is by way of inverting the model and consider tne basic equations (9)–(11) not as a tool to derive the spectral function F(k), and thus the turbulent quantities, but rather as an equation for n_s itself. In fact using the experimentally measured one–dimensional spectrum $E_1(k)$, one can construct the three dimensional E(k), i.e.,

$$2E(k) = k^2 \frac{d^2E_1(k)}{dk^2} - k \frac{dE_1(k)}{dk} \,, \tag{36}$$

the turbulent viscosity $\nu_t(k)$

$$\nu_t(k) = \left[2\gamma \int_k^\infty \frac{F(k)}{k^2}\, dk\right]^{\frac{1}{2}} \,, \tag{37}$$

and finally the rate $\gamma n_c(k)=k^2\nu_t(k)$. Inserting these relations into (9) yields for n_s the expression

$$n_s(k) = \left[\frac{\gamma}{2}\right]^{\frac{1}{2}} \frac{2k^4 I_1(k) - I_2(k)}{k^2 I_1^{\frac{1}{2}}(k)}, \tag{38}$$

where

$$I_1(k) = \frac{E_1(k)}{k}\left[1 - \frac{k}{E_1(k)}\frac{dE_1(k)}{dk}\right] - \int_k^\infty \frac{E_1(k)}{k^2}\,dk\,, \tag{39a}$$

$$I_2(k) = k^3 E_1(k)\left[\frac{k}{E_1(k)}\frac{dE_1(k)}{dk} - 5\right] - k_0^3 E_1(k_0)\left[\frac{k_0}{E_1(k_0)}\frac{dE_1(k)}{dk}\bigg|_{k_0} - 5\right]$$

$$+ 15\int_{k_0}^{k} k^2 E_1(k)\,dk\,, \tag{39b}$$

which can be easily computed once $E_1(k)$ is known experimentally. This procedure yields valuable information on the rate at which energy is being drained from the mean flow into turbulence. At the same time, the k dependence of n_s would help in identifying, or at least narrowing down, the possible types of instabilities that might be candidates. Because of the integration from k to infinity in (39a), it is clear that a successful retrieval of n_s from the experimental data can be carried out only when $E_1(k)$ is known over a large wavenumber interval.

V. SOLUTION OF THE ORR–SOMMERFELD EQUATION

We now proceed to show how the growth rate n_s can be computed from the solution of the well known Orr–Sommerfeld equation,[20–22] whose derivation is briefly sketched below.

mostly to firm up the notation and units employed.

We begin with the Navier–Stokes equations for the total velocity **v** and write the linearized equations for u_i, where as before $v_i = U_i + u_i$. Separating the other variables into mean and fluctuating parts, the latter being indicated by a prime, we obtain with $U_i = \delta_{ix}U(y)$,[22]

$$\frac{du}{dt} + v\frac{dU}{dy} = -\frac{1}{\rho}\frac{dp'}{dx} + \nu\nabla^2 u \tag{40}$$

$$\frac{dv}{dt} = -\frac{1}{\rho}\frac{dp'}{dy} + \nu\nabla^2 v \tag{41}$$

$$\frac{dw}{dt} = -\frac{1}{\rho}\frac{dp'}{dz} + \nu\nabla^2 w \tag{42}$$

where u, v, and w are the x, y, and z components, respectively, of the fluctuating velocity and where $d/dt = \partial/\partial t + U\, d/dx$. In deriving the above equations, the mean flow equations in the linearized limit were also used to eliminate the average pressure. The average density is denoted by ρ. Finally, the incompressibility condition is given by

$$\frac{\partial u}{\partial x} + \frac{\partial v}{\partial y} + \frac{\partial w}{\partial z} = 0\,. \tag{43}$$

Differentiate Eq. (40) with respect to x and Eq. (41) with respect to z, add the resulting equations and use Eq. (43) to obtain an equation containing only the velocity v. Differentiate this result with respect to y. Next, operate with $\partial^2/\partial x^2 + \partial^2/\partial z^2$ on Eq. (42). Using the resulting two equations to eliminate the pressure term, we derive ($'' = d^2/dy^2$)

$$\left[\frac{d}{dt}\nabla^2 - U''(y)\frac{\partial}{\partial x}\right] v(x,y,z) = \nu\nabla^4 v(x,y,z)\,. \tag{44}$$

Now assume that v has the form

$$v(x,y,z) = v(y) \exp [i(k_x x + k_z z - k_x ct)] . \tag{45}$$

With the notation

$$k_\perp^2 = k_x^2 + k_z^2 , \tag{46}$$

Eq. (44) becomes the well known Orr–Sommerfeld equation,[20–23]

$$\frac{\nu}{ik_x}\left[\frac{d^2}{dy^2} - k_\perp^2\right]^2 v(y) = (U(y)-c)\left[\frac{d^2}{dy^2} - k_\perp^2\right] v(y) - U''(y)v(y) . \tag{47}$$

It is convenient to write this equation in terms of dimensionless quantities. Measuring lengths in terms of the channel half–width, D, and velocities in terms of the laminar centerline mean velocity, U_0^L, we introduce the following dimensionless variables:

$$\alpha = k_x D, \quad \tilde{\alpha} = k_\perp D, \quad \mathcal{y} = y/D, \quad \mathcal{U} = U/U_0^L, \quad \mathcal{c} = c/U_0^L . \tag{48}$$

Eq. (47) then becomes

$$\frac{1}{i\alpha R_L}(\mathcal{D}^2 - \tilde{\alpha}^2)^2 v(\mathcal{y}) = \left[\mathcal{U}(\mathcal{y}) - \mathcal{c}\right](\mathcal{D}^2 - \tilde{\alpha}^2) v(\mathcal{y}) - U''(\mathcal{y}) v(\mathcal{y}) , \tag{49}$$

where $\mathcal{D} = d/d\mathcal{y}$ The mean flow $\mathcal{U}(\mathcal{y})$ at this point is still arbitrary. For a Poiseiulle flow, $\mathcal{U}(\mathcal{y}) = 1-\mathcal{y}^2$ is used and the boundary conditions $v = dv/d\mathcal{y} = 0$ are imposed at $\mathcal{y} = \pm 1$. If we further define $\tilde{R}_L$ by $\alpha R_L = \tilde{\alpha}\tilde{R}_L$, we obtain

$$\tilde{R}_L = \frac{R_L k_x}{(k_x^2 + k_z^2)^{\frac{1}{2}}} = R_L \cos\phi\,, \tag{50}$$

then the solution of Eq. (49) yields for a given $\tilde{R}_L$ the complex eigenvalue c as a function of $\tilde{\alpha}$. Actually, for a given $\tilde{\alpha}$, there is a large number of discrete complex eigenvalues c. However, only one of the c's has a positive imaginary part for some range of $\tilde{\alpha}$ which leads to growth of the instability (see Eq. 45). Defining the growth rate $n_s = k_x \mathrm{Im}(c)$ (where Im stands for the imaginary part of the enclosed function), the solution of Eq. (49) yields

$$n_s = \frac{U_0^L}{D}\,\tilde{\alpha}\,\mathrm{Im}(c)\cos\phi \quad \text{vs.} \quad \tilde{\alpha}, \tag{51}$$

for a given value of $\tilde{R}$. One can easily see that the maximum value of n_s (the most dangerous mode) corresponds to taking $\cos\phi = 1$, i.e., $k_z = 0$. To compare our results with experimental data, we need to change the velocity normalization from the undisturbed centerline mean velocity, U_0^L, to the experimental centerline mean velocity, U_0. This is done by multiplying Eq. (51) by $U_0/U_0^L = R_{exp}/R_L$. Hence, the desired growth rate is

$$\frac{n_s}{n_*} \text{ vs. } k_\perp D\,, \quad \text{where } n_* = \frac{U_0}{D}\,, \tag{52}$$

for different values of R_L or, equivalently, of $R_{exp} = U_0 D/\nu$.

VI. DETERMINATION OF k_y^2

Equation (52) is not yet the final result, for it gives n_s as a function of $k_\perp$. However, since homogeneity has been assumed in the application of the DIA and in the construction of the GISS model, they require the knowledge of the growth rate as a function of the total

wavenumber, k. Channel flow is inhomogeneous in the direction perpendicular to the channel walls (the y–direction) so that an application of the model equations requires the construction of a wavenumber in the y–direction, i.e., $k_y = k_y(k_\perp)$. The application of a model which assumes homogeneity to a manifestly inhomogeneous flow may be criticized on first principles, yet we have learned from Leslie's work[12] that the problem is analytically a very difficult one and trade–offs must be made to simplify it in order to make it solvable. We have kept as much as possible of the essential physics in the model intact, consistent with the necessity of keeping the problem solvable. One of these trade–offs is our inability to describe the variation in the details of the flow in the y–direction. All of our calculated bulk properties represent an average of these properties over the inhomogeneous direction. We therefore proceed to find a suitable relationship between k_y and $k_\perp$. Following the original work of Synge,[20] we multiply the O–S equation (47) from the left by v^* and integrate the result over y from –D to +D. Separating the real and imaginary parts, one obtains for the growth rate, $n_s = k_x \mathrm{Im}(c)$, the expression

$$n_s = \frac{k_x \mathrm{Im}(Q)}{I_1^2 + k_\perp^2 I_0^2} - \nu \frac{I_2^2 + 2k_\perp^2 I_1^2 + k_\perp^4 I_0^2}{I_1^2 + k_\perp^2 I_0^2}, \tag{53}$$

where

$$\mathrm{Im}(Q) = -\frac{1}{2}\int_{-D}^{D} U' \left[k_x(uv^* + u^*v) + k_z(vw^* + v^*w)\right] dy \tag{54}$$

and

$$I_n^2 = \int_{-D}^{D} \left|\frac{d^n v}{dy^n}\right|^2 dy . \tag{55}$$

In deriving Eq. (54), we have extended Eq. (45) to u and w and have used Eq. (43) in the form $dv/dy = -i(k_x u + k_z w)$.

Equations (53)–(55) have a simple physical interpretation. The first term is a "production term", since it provides the interaction between the shear $s = U'(y)$ in the mean flow and the Reynolds stress tensor: it gives a positive contribution to n_s, see Eq. (1). The second term is proportional to the viscosity, ν, and is always negative. It must clearly dominate at very large wavenumbers where the only remaining physical mechanism is kinematic viscosity. As we know, the latter enters the Navier–Stokes equations in the form $-\nu k^2$. On that basis, we shall therefore identify the coefficient of ν with k^2, i.e.,

$$k^2 = k_y^2 + k_\perp^2 = \frac{I_2^2 + 2k_\perp^2 I_1^2 + k_\perp^4 I_0^2}{I_1^2 + k_\perp^2 I_0^2}, \tag{56}$$

which, after some rearrangements, yields the desired result

$$k_y^2 = \frac{I_2^2 + k_\perp^2 I_1^2}{I_1^2 + k_\perp^2 I_0^2}, \tag{57}$$

which we shall use to generate the wavenumber k_y from the solutions of the O–S equation. For the fastest growing mode ($\cos\phi = 1$), (57) becomes

$$k_y^2 = \frac{\int_{-1}^{1} (u^* \mathcal{D}^2 u + v^* \mathcal{D}^2 v)\, dy}{\int_{-1}^{1} (u^* u + v^* v)\, dy}. \tag{58}$$

This result is intuitively appealing since k_y^2 is found to be the average of the operator d^2/dy^2 over the flow in the y–direction.

VII. THE RESULTS FOR $n_s(k)$ AND k_y

We have solved the O–S equation (49) for four values of R_{exp}: 1.23, 2.86, 3.08, and 5 ($\times 10^4$). The first three values correspond to the experimental values of Laufer[1] and Hussain and Reynolds.[4] In Table II, we present the values of $n_s(k)$ in units of n_*, Eq. (52), as a function of the dimensionless wavenumber kD and in Table III we give the values of k_y vs. $k_\perp$. In Fig.(2), we plot n_s/n_* vs. kD for different values of the Reynolds number.

VIII. SOLUTIONS OF THE TURBULENCE EQUATIONS

The function $n_s(k)$ was used to solve both the DIA and the GISS models, Eqs. (12) and (14)–(15). In each case, we computed several quantities of interest that we discuss below.

1) Turbulent energy spectral function, F(k). In Fig. (3) we plot

$$F(k)/F_* \text{ vs. } kD\,, \qquad F_* = U_0^2 D = (\nu^2/D)\, R_{exp}^2\,, \tag{59}$$

calculated using the GISS model. In Fig. (4), we compare the GISS and DIA results.

2) The energy $\epsilon(k)$. In Fig. (5) we plot the quantity

$$\epsilon(k)/\epsilon_* \text{ vs. } kD\,, \qquad \epsilon_* = U_0^3/D = (\nu^3/D^4)\, R_{exp}^3\,, \tag{60}$$

where $\epsilon(k)$ is defined in (5) and (7). (The physical units of ϵ are erg g^{-1} sec^{-1}.)

3) The turbulent viscosity, $\nu_t(k)$. In Fig. (6) we plot

$$\nu_t(k)/\nu_* \quad \text{vs.} \quad kD\,, \quad \nu_* = U_0 D = \nu R_{exp}\,, \tag{61}$$

where $\nu_t(k)$ is the turbulent viscosity defined in (8). The largest value of the turbulent viscosity is attained at $k=k_0$, where k_0 is the smallest allowed wavenumber. Taking the limit $k \to k_0$ in Eq. (5), we obtain

$$\nu_t(k_0) = \frac{n_s(k_0)}{k_0^2}\,. \tag{62}$$

4) One dimensional spectra. Both Laufer[1] and Hussain and Reynolds[4] present their experimental results in terms of the one dimensional spectral energy function defined in terms of the three dimensional F(k) as follows (see Ref. 10, Eqs. 3.72, 3.48, 3.47)

$$E_1(k_1) = \frac{1}{2}\int_{k_1}^{\infty} k^{-1} F(k)\,(1-k_1^2/k^2)\,dk\,. \tag{63}$$

We have computed $E_1(k_1)$ for the case corresponding to the experimental condition in the Hussain and Reynolds paper, i.e., $R_{exp} = 28600$, $U_o = 1350$ cm sec^{-1}, $D = 3.18$ cm. The results are presented in Fig. (7).

On the other hand, Laufer[1] presents his experimental data in terms of the function

$$F_{\overline{u}^2}(n) = \frac{2\pi}{U_0} E_1(k_1) \left[\int_0^{\infty} E_1(k_1)\,dk_1\right]^{-1}\,, \tag{64}$$

where $2\pi n = k_1 U_0$. The comparison between Laufer's measured spectrum (R_{exp}= 30800. U_0 = 728 cm sec^{-1}, D = 6.35 cm) and the theoretical results is presented in Fig. (8).

5) Turbulent velocities and scales of turbulence. Laufer[1] and Hussain and Reynolds[4] also provide experimental data for other quantities of interest, namely

a) turbulent energy,

$$< u^2 > = \int_0^\infty F(k)\, dk\ , \tag{65}$$

b) turbulent velocity,

$$<u_x^2>^{\frac{1}{2}} = <u_y^2>^{\frac{1}{2}} = <u_z^2>^{\frac{1}{2}} = \left[\frac{<u^2>}{3}\right]^{\frac{1}{2}}\ . \tag{66}$$

c) Taylor microscale λ_x,

$$\lambda_x^2 = \int_0^\infty E_1(k_1)\, dk_1 \left[\int_0^\infty k_1^2\, E_1(k_1)\, dk_1\right]^{-1}\ , \tag{67}$$

d) turbulence macroscale, Λ_x,

$$\Lambda_x = \frac{\pi}{2} E_1(0) \left[\int_0^\infty E(k)\, dk\right]^{-1}\ , \tag{68}$$

e) Kolmogoroff scale, l_0,

$$l_0 = (\nu^3/\epsilon)^{1/4}\ . \tag{69}$$

In Table IV, we present $<u^2>$ in units of U_0^2, $<u_x^2>^{\frac{1}{2}}$ in units of U_0, $\nu_t=\nu_t(k_0)$ in units of U_0D, ϵ in units of U_0^3/D, and λ_x, Λ_x, and l_0 in units of D. Experimental data are included when available.

IX. PRESSURE FLUCTUATIONS IN A TURBULENT CHANNEL FLOW

We begin by considering that in an incompressible fluid, the pressure $p(\mathbf{x})$ is given by the solution of the Poisson's equation

$$\nabla^2 p(\mathbf{x}) = -\rho \frac{\partial^2 v_i(\mathbf{x}) v_j(\mathbf{x})}{\partial x_i \partial x_j}, \tag{70}$$

where $\mathbf{v}(\mathbf{x})$ is the total velocity, ρ is the constant density, and the summation convention has been employed. If, as usual, one splits v_i into a fluctuating part u_i and a mean field U_i, the right hand side of (70) is seen to contain three contributions: a term in u_iu_j, one in the form u_iU_j, and one in U_iU_j. Following Kraichnan,[28,29] we shall assume that the cross term is much smaller than the other two so that from the solution of (70), one can construct the fluctuating pressure, i.e.,

$$\frac{<p^2>}{\rho^2} = \int d^3\mathbf{k}\, [\Pi_{T-T}(\mathbf{k}) + \Pi_{T-M}(\mathbf{k})] \equiv \int d^3\mathbf{k}\, \Pi(\mathbf{k}), \tag{71}$$

where T–T indicates the contribution arising from the turbulence–turbulence interaction and T–M indicates the one arising from the interaction between the turbulence and the mean flow. It is a known fact, which we have verified numerically, that

$$\Pi_{T-M} >> \Pi_{T-T}. \tag{72}$$

The expression for Π_{T-T} was first evaluated by Batchelor.[30] The result is

$$4\pi\,\Pi_{T-T}(\mathbf{k}) = \iint E(k')E(k-k')\,\frac{\sin^4\theta}{|\mathbf{k}-\mathbf{k}'|^4}\,k'^2dk'\sin\theta d\theta\,. \tag{73}$$

The expression for Π_{T-M} is much more difficult to compute. To treat the physical problem under consideration, we need an expression that depends not only on $\mathbf{k}$ but also on the coordinate variable across the channel of finite width Δ, i.e.

$$\Pi_{T-M}(\mathbf{k}) \rightarrow \Pi_{T-M}(\mathbf{k},x_2;\Delta)\,. \tag{74}$$

The only expression for Π_{T-M} available in the literature is one due to Kraichnan[29] (his Eq. 5.20), which yields the pressure at the lower boundary of a semi–infinite medium, (a flat plate) i.e.,

$$\Pi_{T-M}(\mathbf{k},0;\infty)\,. \tag{75}$$

Since we plan to study the propagation of an electromagnetic beam in a channel flow, Kraichan's expression is not applicable to our case. We shall therefore derive the expression for $\Pi_{T-M}(\mathbf{k},x_2) \equiv \Pi_{T-M}(\mathbf{k},x_2;\Delta)$.

Since in the case of a channel flow, two directions, say x_1 and x_3, in the plane of the mean flow can be considered to be homogeneous, one can perform a Fourier transform of (70) on the variables x_1, x_3, and ω. Eq. (70) then becomes

$$\frac{\partial^2 p(x_2,\kappa,\omega)}{\partial x_2^2} - \kappa^2 p(x_2,\kappa,\omega) = -\,T(x_2,\kappa,\omega)\,, \tag{76}$$

where $\kappa^2 = k_1^2 + k_3^2$, and

$$p(x_2,\kappa,\omega) = (2\pi)^{-3/2} \int p(\mathbf{x},t) e^{-i(k_1x_1+k_3x_3-\omega t)} dx_1 dx_3 dt \,. \tag{77}$$

Eq. (76) is a second order, inhomogeneous differential equation whose solution can be written as

$$2\kappa p(x_2,\kappa,\omega) = \int_a^{x_2} dx_2' \, e^{-\kappa(x_2-x_2')} T(x_2',\kappa,\omega) - \int_b^{x_2} dx_2' \, e^{\kappa(x_2-x_2')} T(x_2',\kappa,\omega) \,. \tag{78}$$

The two constants of integration a and b must be determined by imposing the boundary conditions

$$\frac{d}{dx_2} p(x_2,\kappa,\omega)\Big|_{x_2=0,\Delta} = 0 \,, \tag{79}$$

since the fluid is bounded by two walls at $x_2 = 0$ and $x_2 = \Delta = 2D$. The final result is

$$p(x_2,\kappa,\omega) = \int_0^{\Delta} dx_2' \, g_2(x_2,x_2';\kappa) T(x_2') - \int_0^{x_2} dx_2' \, g_1(x_2,x_2';\kappa) T(x_2') \,, \tag{80}$$

where, for the sake of simplicity, we have explicitly written only the x_2 dependence of T. i.e., $T(x_2) = T(x_2,\kappa,\omega)$, and where we have defined two function g_1 and g_2 as

$$\kappa g_1(x_2,x_2';\kappa) = \sinh \kappa(x_2-x_2') \tag{81}$$

$$\kappa g_2(x_2,x_2';\kappa) = \frac{\cosh \kappa x_2}{\sinh \kappa\Delta} \cosh \kappa(\Delta-x_2') \,. \tag{82}$$

By taking the limit $\Delta \to \infty$ and $x_2 \to 0$, (80) reduces to Eq. (3.9) of Kraichnan.[29] (In the case $x_2=0$ and nonzero Δ, Eq. (80) does not reduce to Eq. 3.11 of Kraichnan[29] since the latter is missing a factor of 2 in front of the second term.) Eq. (80) is the basic ingredient of our calculations since it gives the value of the fluctuating pressure at any given point in a channel of full width $\Delta=2D$. From (80) we obtain, with a slight change of notation,

$$|p(x_2,\kappa,\omega)|^2 = \int_0^\Delta dx \int_0^\Delta dy\, g_2(x_2,x;\kappa)g_2(x_2,y;\kappa)\langle T^*(x,\kappa,\omega)T(y,\kappa,\omega)\rangle$$

$$-2\int_0^\Delta dx \int_0^{x_2} dy\, g_1(x_2,y;\kappa)g_2(x_2,x;\kappa)\langle T^*(x,\kappa,\omega)T(y,\kappa,\omega)\rangle$$

$$+\int_0^{x_2} dx \int_0^{x_2} dy\, g_1(x_2,x;\kappa)g_1(x_2,y;\kappa)\langle T^*(x,\kappa,\omega)T(y,\kappa,\omega)\rangle\,, \qquad (83)$$

where the star denotes complex conjugation and the angular brackets denote an ensemble average.

As is well known, the largest contribution to $T(x_2)$ comes from the interaction of the turbulent field with the mean flow, i.e.

$$T(\mathbf{x},t) = 2\rho s(x_2)\frac{\partial U_2}{\partial x_1}\,, \qquad (84)$$

where the shear $s(x_2)$ is given by

$$s(x_2) = \frac{\partial U_1(x_2)}{\partial x_2}\,, \tag{85}$$

so that

$$<T(x,t)T(x',t')> = S(x_2,x_2',x_1-x_1',x_3-x_3',t-t')$$

$$= -4\rho^2\, s(x_2)s(x_2')\,\frac{\partial}{\partial\zeta_1^2}\,R_{22}(x_2,x_2',\zeta_1,\zeta_3,t)\,, \tag{86}$$

where it has been explicitly indicated that in the directions x_1 and x_3 the fluid is homogeneous, R_{22} is the two point velocity correlation function, $\zeta_1 = x_1' - x_1$, and $\zeta_3 = x_3' - x_3$. Taking now

$$R_{22}(x_2,x_2',\zeta_1,\zeta_3,t) = (2\pi)^{-3/2}\int d^2\kappa d\omega\, e^{i(\kappa\cdot\zeta+\omega t)}\, R_{22}(x_2,x_2',\mathbf{k},\omega) \tag{87}$$

and using an analogous expansion for S, we have

$$S(x_2,x_2',\kappa,\omega) = 4\rho^2\, s(x_2)s(x_2')\,\kappa_1^2\, R_{22}(x_2,x_2',\kappa,\omega)\,. \tag{88}$$

The relation between $<T^*(x,\kappa,\omega)T(y,\kappa,\omega)>$ in (83) and the quantity $S(x_2,x_2,\kappa,\omega)$ is[29] $<T^*(x,\kappa,\omega)T(y,\kappa,\omega)> = (2\pi)^{-3/2}\, S(x_2,x_2',\kappa,\omega)$. Using the reality of $R_{22}(\mathbf{x},t)$, we write

$$R_{22}(x_2,x_2',\kappa,\omega) = \frac{(2\pi)^{\frac{1}{2}}}{\Delta}\sum_{n=-\infty}^{\infty}{}'\cos k_2^{(n)}(x_2-x_2')\, R_{22}(\mathbf{k},\omega)\,, \tag{89}$$

where $k_2^{(n)} = 2\pi n/\Delta$. Eqs. (86)–(89) are substituted in (83) and the result is integrated over all ω. Using the relations

$$\int_{-\infty}^{\infty} R_{22}(\mathbf{k},\omega)\, d\omega = (2\pi)^2\, \Phi_{22}(\mathbf{k}) \tag{90}$$

$$\Phi_{22}(\mathbf{k}) = \frac{E(k)}{4\pi k^4}\,\kappa^2\,, \tag{91}$$

where E(k) is the velocity spectrum for homogeneous turbulence, and where

$$\langle p^2(x_2)\rangle = \int |p(x_2,\mathbf{k},\omega)|^2\, d^2\kappa d\omega\,, \tag{92}$$

we obtain, after a series of lengthy integrations over the variables x and y in (83), the final result

$$\frac{\langle p^2(x_2)\rangle}{\rho^2} = \int d^3\mathbf{k}\, \Pi(\mathbf{k},x_2)\,, \tag{93}$$

where

$$\Pi(\mathbf{k},x_2) = \frac{s_0^2}{\pi}\frac{2\pi}{\Delta}\sum_{n=-\infty}^{\infty}\delta(k_2-k_2^{(n)})\,\frac{E(k)}{k^4}\,\frac{k_1^2k_3^2}{k^4}\left[\Gamma_1^2(\mathbf{k},x_2)+\Gamma_2^2(\mathbf{k},x_2)\right] \tag{94}$$

$$\Gamma_1(\mathbf{k},x_2) = \frac{\cosh\,\kappa(\frac{1}{2}\Delta-x_2)}{\sinh\,\frac{1}{2}\kappa\Delta} + \frac{\kappa}{k_2^{(n)}}\left[1-2\frac{x_2}{\Delta}\right]\sin k_2^{(n)}x_2 - \frac{4\kappa}{k^2\Delta}\cos k_2^{(n)}x_2 \tag{95}$$

$$\Gamma_2(\mathbf{k},x_2) = \frac{2}{k_2\Delta}\left[1-2\frac{\kappa^2}{k^2}\right]\frac{\sinh\,\kappa(\frac{1}{2}\Delta-x_2)}{\cosh\,\frac{1}{2}\kappa\Delta} + \frac{\kappa}{k_2^{(n)}}\left[1-2\frac{x_2}{\Delta}\right]\cos k_2^{(n)}x_2 + \frac{4\kappa}{k^2\Delta}\sin k_2^{(n)}x_2\,. \tag{96}$$

with $\delta(x)$ the Dirac delta function. To be consistent with the spirit of the model adopted in this paper, the velocity profile used in performing the integrations that lead to (93) was $U(x_2) = s_0 x_2(1 - x_2/\Delta)$, where $s_0 = \tau_0/\nu$. This gives for the shear

$$s(x_2) = s_0\left[1 - \frac{2}{\Delta}x_2\right]. \tag{97}$$

However, it is clear that the above formalism is valid for any shear.

Using the spectral functions E(k) derived from the DIA and GISS models, we have computed the pressure spectral function $\Pi(k)$ and then integrated over all wavevectors **k**. The resulting pressures, in units of ρU_τ^2, are presented in Figs. (9) and (10). As one can see, for $R_{exp} = 5000$, the calculated value of the pressure at the wall is 6.31, while experiments[31] and direct numerical simulation[32] yield a lower value, i.e. 3.22, the discrepancy being due most likely to anisotropy effects (see XI).

X. PROPAGATION OF ELECTROMAGNETIC WAVES IN A TURBULENT CHANNEL FLOW

An important application of the previous formalism is to the case of propagation of a laser beam through a turbulent channel flow medium. Of primary importance is, for example, the evaluation of the degree of attenuation in the beam intensity I. Using the formalism developed by Hogge et al.,[33] the total beam intensity I, as a function of the coordinates x_0 and y_0 in the plane perpendicular to the direction of propagation, is given by

$$I(x_0,y_0) = \frac{A_0^2}{(\lambda f)^2}\exp(-\sigma_\phi^2)\int dx_1 dx_2 dy_1 dy_2 \exp\left[C_\phi(\rho) - g - ip/f\left[x_0(x_1-x_2) + y_0(y_1-y_2)\right]\right] \tag{98}$$

where

$$w_{1g}^2 \equiv x_1^2 + x_2^2 + y_1^2 + y_2^2 , \tag{99}$$

$$\rho^2 \equiv (x_1-x_2)^2+(y_1-y_2)^2 , \tag{100}$$

$$p \equiv \frac{2\pi}{\lambda} . \tag{101}$$

Here, λ is the wavelength, f the focal distance, and w_1 the spot size. In Eq. (98), $C_\phi(\rho)$ is the phase autocorrelation function and σ_ϕ^2 its value at $\rho = 0$. By separating the integrand in (98) so as to exhibit the coherent and incoherent parts of the total intensity, one can then evaluate the corresponding powers obtained by integrating the intensity over the variables x_0 and y_0. A simple integration then gives the exact result

$$P = P_{inc}/P_{total} = 1 - \exp(-\sigma_\phi^2) , \tag{102}$$

which is often written as

$$P = \frac{\sigma_\phi^2}{1 + \sigma_\phi^2} , \tag{103}$$

since in most cases σ_ϕ^2 is smaller than unity. The quantity $\sigma_\phi^2 = C_\phi(0)$ is defined as[34]

$$\sigma_\phi^2 = p^2 \int d^3k \int_0^L d\xi' \int_0^L d\xi'' \cos\left[k_2(\xi'-\xi'')\right]\cos\left[\omega(L-\xi')\right]\cos\left[\omega(L-\xi'')\right] \Phi_n(k,x',x'') \tag{104}$$

where

$$\omega = \frac{k_\perp^2}{2p}, \qquad \kappa^2 = k_1^2 + k_3^2, \qquad k^2 = k_2^2 + \kappa^2 \tag{105}$$

the ξ' and ξ'' integrations are over the the photon optical path of length L. which is related to the full channel width 2D, $x' = (2D/L)\xi'$, and $x'' = (2D/L)\xi''$. One of the integrations over optical path in (104) can be done by changing variables to sum and difference coordinates, $(\xi'+\xi'')/2$ and $\xi'-\xi''$. We then assume that Φ_n is a locally isotropic field, i.e., a function only of the sum coordinates, so that the integration over the difference coordinates can be done analytically.

The function Φ_n is defined as the spectral function of the square of the refractive index fluctuations, i.e., for mean flow in the x_1 direction with the coordinate system oriented such that x_2 is the coordinate variable spanning the channel with $0 \le x_2 \le \Delta = 2D$. we have

$$\langle n'^2(x_2)\rangle = \int d^3\mathbf{k}\, \Phi_n(\mathbf{k},x_2)\,, \tag{106}$$

where we have taken[25]

$$n = 1 + n' = 1 + \alpha p, \qquad \alpha = 7.9 \times 10^{-8} g(\lambda)/T\,. \tag{107}$$

Here the pressure p is measured in c.g.s. units and the temperature T in K. The slight dependence on the wavelength λ is represented by the function $g(\lambda)$, where $g(\lambda=1\mu) = 1$. $g(\lambda=0.5\mu) = 1.02$, and $g(\lambda=0.2\mu) = 1.18$. It then follows that

$$<n'^2(x_2)> = (\alpha\rho)^2 \frac{<p^2(x_2)>}{\rho^2} = \int \Phi_n(\mathbf{k}.x_2)\, d^3\mathbf{k}\,. \qquad (108)$$

where ρ is the density in cgs units. Using (71), it follows that

$$\Phi_n(\mathbf{k}.x_2) = (\alpha\rho)^2\, \Pi(\mathbf{k}.x_2)\,. \qquad (109)$$

1) The quantity $\rho\alpha U_0^2$

Using the equation of state and the sound speed c_s

$$p = \frac{kN_A}{\mu}\rho T = \frac{8.32 \times 10^7}{\mu}\rho T\,, \qquad c_s^2 = \gamma\frac{p}{\rho}\,, \qquad (110)$$

where k is Boltzmann's constant, N_A is Avogadro's number, μ the molecular weight (gm/mole), and γ the ratio of specific heats, we derive using (107)

$$\rho\alpha U_0^2 = \gamma_* M^2\,, \qquad (111)$$

where the constant γ_* (ρ is in c.g.s. units) and the Mach number M are defined as

$$\gamma_* \equiv 6.5696\,\gamma\frac{\rho}{\mu}\,, \qquad M \equiv \frac{U_0}{c_s}\,. \qquad (112)$$

2) The results

In Table V, we present the values of 10^2P, Eq. (102), calculated using Eqs. (104), (109), and (94). The spectral function E(k) is calculated using both the GISS model and

the DIA. For each entry, R_{exp} and M, the corresponding U_0, D (the channel half–width), and L (optical path) can be computed from the following relations (p in atmospheres and ρ in c.g.s. units)

$$U_0(\text{cm/sec}) = c_s M = 10^3 M\,(\gamma p/\rho)^{\frac{1}{2}} \tag{113}$$

$$D(\text{cm}) = \frac{\nu}{U_0} R_{exp}, \quad L(\text{cm}) = 2(1 + n_r^2)^{\frac{1}{2}}\, D(\text{cm}), \tag{114}$$

The values of the viscosity ν (in $\text{cm}^2\ \text{s}^{-1}$), density ρ (in gm cm^{-3}), and the refractive index n_r are given in Table V. A plot of $10^2 P$ versus the Mach number is displayed in Fig. (11) for $\Delta = 2$, 3, and 5 mm.

XI. ANISOTROPY

As mentioned at the end of Section IX, we believe, on the basis of Kraichnan's work,[28] that the reason for the discrepancy between the calculated and measured values of the pressure fluctuations at the wall is the lack in our calculation of the inclusion of anisotropy effects induced by the mean flow. This is also believed to be the cause of the discrepancy between the calculated and observed one–dimensional energy spectra. Kraichnan presented a simple model for an elongated eddy structure by introducing a (constant) scale change in the direction of the mean flow. This simple model will be adopted here in order to judge what qualitative effect anisotropy would have on the one–dimensional energy spectrum.

Following Kraichnan,[28] we introduce a transformation of scale defined by

$$x_1' = \alpha x_1 , \qquad x_2' = x_2 , \qquad x_3' = x_3 , \tag{115a}$$

for the spatial coordinate variables where 1 is the streamwise direction and 2 is the direction across the channel, and

$$k_1' = \frac{k_1}{\alpha} , \qquad k_2' = k_2 , \qquad k_3' = k_3 , \tag{115b}$$

for the wavenumber variables, where α is a constant scale factor. The primed variables in (115), i.e., those for which the scales are stretched in the streamwise direction, are the physical variables. Since we only know E(k) for the isotropic case (in which there is no stretching), we derive a relationship between the velocity covariance tensors in the primed and unprimed systems. For homogeneous and isotropic turbulence, the velocity correlation function $\Phi_{ij}(\mathbf{k})$ is given by (Ref. 15, Eq. 3.4.12)

$$\Phi_{ij}(\mathbf{k}) = \frac{E(k)}{4\pi k^2}\left[\delta_{ij} - \frac{k_i k_j}{k^2}\right] , \tag{116}$$

where δ_{ij} is the Kronecker delta, E(k) is the energy spectrum, and

$$\langle u^2 \rangle = \int d^3\mathbf{k}\, \Phi_{ii}(\mathbf{k}) . \tag{117}$$

The velocity covariance is a second rank covariant tensor. Applying the coordinate change (115b) to $\Phi_{ij}(\mathbf{k})$ yields

$$\Phi_{11}(\mathbf{k}') = N\alpha^2 \Phi_{11}(\mathbf{k}) \tag{118}$$

$$\Phi_{1j}(\mathbf{k}') = N\alpha \Phi_{1j}(\mathbf{k}) , \qquad j \neq 1 \tag{119}$$

$$\Phi_{ij}(\mathbf{k}') = N\Phi_{ij}(\mathbf{k}) , \qquad i,j \neq 1 , \tag{120}$$

for the velocity covariance in the $\mathbf{k}'$ coordinate system, where the normalization coefficient N has been added to these expressions to insure that the mean kinetic energy is identical to that of the original flow. The new correlation tensor now describes a flow for which all lengths and velocities are elongated by a factor α in the x_1 direction. To calculate N, note that the kinetic energy (per unit mass) in the new coordinate system is

$$\tfrac{1}{2} \int \Phi_{ii}(\mathbf{k}') \, d^3\mathbf{k}' = \tfrac{1}{2} \frac{N}{\alpha}(\alpha^2 R_{11} + R_{22} + R_{33}) , \tag{121}$$

where $R_{ii} \equiv \int \Phi_{ii}(\mathbf{k}) \, d^3\mathbf{k}$ (no sum on the indices). To insure that the mean kinetic energy is identical to the original flow, (121) is equated to $\frac{1}{2}(R_{11} + R_{22} + R_{33})$. For isotropic R_{ii}, the resulting equation is solved for N and we find that

$$N = \frac{3\alpha}{\alpha^2+2} . \tag{122}$$

a) One–Dimensional Spectra

The one–dimensional energy spectrum in the physical coordinate system is given by

$$E_1(k_1') = 2 \int d^2\boldsymbol{\kappa}' \, \Phi_{11}(\mathbf{k}') , \tag{123}$$

where $\kappa'^2 = k_2'^2 + k_3'^2$. After changing the variable of integration to $k'^2 = \alpha^2 k_1'^2 + \kappa'^2$ and taking $k' \to k$ in the integral for ease of notation, the result for the one–dimensional energy spectrum in the physical variables is

$$E_1(k_1') = \frac{3\alpha^3}{\alpha^2+2} \int_{\alpha k_1'}^{\infty} \frac{E(k)}{k} \left[1 - \frac{\alpha^2 k_1'^2}{k^2}\right] dk \,. \tag{124}$$

Fig. (12) is a plot of the observed $E_1(k_1')$ for R_{exp}=30800 and that calculated using the DIA result. (Actually, we plot $F_{\overline{u}^2}(n)$, see Eq. (64).) The scale factor α is a free parameter and Fig. (12) displays the results for $\alpha = 1$, 4, and 8.

This procedure has provided a qualitative improvement over the $\alpha = 1$ result. The turnover of the spectrum, originally occurring at $n \sim 200\ s^{-1}$, has moved to frequencies (i.e., wavenumbers) beyond the lowest observed, in concert with the observations. Naturally, it is not to be expected that the procedure presented here would provide a perfect fit to the data since the mean flow may not affect all scale lengths in the same way. However, the results do suggest that accounting for anisotropy considerably improves the fitting of the one–dimensional spectra.

b) Pressure Fluctuations

For the anisotropic case, the calculation of the pressure fluctuations is similar to that done in Section IX. For the amplitude of the pressure fluctuations, we write

$$\frac{\langle p^2(x_2')\rangle}{\rho^2} = \int d^3\mathbf{k}'\ \Pi(\mathbf{k}',x_2') \,, \tag{125}$$

$$\Pi(\mathbf{k}',x_2') = 4s_0^2 \frac{2\pi}{\Delta} \sum_{n=-\infty}^{\infty} \delta(k_2'-k_2^{(n)}) \frac{k_1'^2}{\kappa'^2} \frac{k_2'^2}{k'^4} \Phi_{22}(\mathbf{k}') \left[\Gamma_1^2(\mathbf{k}',x_2') + \Gamma_2^2(\mathbf{k}',x_2')\right] \tag{126}$$

$$\Gamma_1(\mathbf{k}',x_2') = \frac{\cosh \kappa'(\frac{1}{2}\Delta - x_2')}{\sinh \frac{1}{2}\kappa'\Delta} + \frac{\kappa'}{k_2'}\left[1 - 2\frac{x_2'}{\Delta}\right] \sin k_2'x_2' - \frac{4\kappa'}{k'^2\Delta} \cos k_2'x_2' \tag{127}$$

$$\Gamma_2(\mathbf{k}',x_2') = \frac{2}{k_2'\Delta}\left[1 - 2\frac{\kappa'^2}{k'^2}\right]\frac{\sinh\,\kappa'(\frac{1}{2}\Delta - x_2')}{\cosh\,\frac{1}{2}\kappa'\Delta} + \frac{\kappa'}{k_2'}\left[1 - 2\frac{x_2'}{\Delta}\right]\cos k_2'x_2'$$
$$+ \frac{4\kappa'}{k'^2\Delta}\sin k_2'x_2' \,, \qquad (128)$$

with $\delta(x)$ the Dirac delta function, $k_2^{(n)} = 2\pi n/\Delta$, and $\kappa'^2 = k_1'^2 + k_3'^2$. In (125)–(128), the integration variables and position variable have been written as $\mathbf{k}'$ and x_2', respectively, in order to emphasize that these are the physical coordinates, i.e., those stretched in the streamwise direction. Although we only know E(k) in terms of wavenumbers from which the stretching has been removed, we do know how to relate $\Phi_{ij}(\mathbf{k}')$ to $\Phi_{ij}(\mathbf{k})$. Now change variables in the integral from $\mathbf{k}'$ to $\mathbf{k}$. Working in the coordinate system defined by

$$k_1 = k\sin\theta\cos\phi\,, \qquad k_2 = k\cos\theta\,, \qquad k_3 = k\sin\theta\sin\phi\,, \qquad (129)$$

the quantities κ'^2 and k'^2 are given by

$$\kappa'^2 = k^2\sin^2\theta\,(1 - \frac{\alpha^2-1}{\alpha^2}\cos^2\phi) \equiv k^2 f(\phi)\sin^2\theta\,, \qquad (130)$$

$$k'^2 = k^2\,(1 - \frac{\alpha^2-1}{\alpha^2}\sin^2\theta\cos^2\phi) \equiv k^2 g(\theta,\phi)\,. \qquad (131)$$

Using $d^3\mathbf{k}' = d^3\mathbf{k}/\alpha$, we have from (125)

$$\frac{<p^2(x_2;\alpha)>}{\rho^2} = \frac{1}{\alpha}\int d^3\mathbf{k}\;\Pi(\mathbf{k},x_2;\alpha)\,, \qquad (132)$$

where

$$\Pi(\mathbf{k},x_2;\alpha) = \frac{s_0^2}{\pi^2}\frac{N}{\alpha^2}\frac{2\pi}{\Delta}\sum_{n=-\infty}^{\infty}\delta(k_2-k_2^{(n)})\frac{E(k)}{k^4}\frac{\sin^2\theta\cos^2\phi}{f(\phi)g^2(\theta,\phi)}\frac{k_2^2}{k^2}$$

$$\times\,(\Gamma_1^2(\mathbf{k}',x_2) + \Gamma_2(\mathbf{k}',x_2))\,, \tag{133}$$

and Γ_1 and Γ_2 are given by (127) and (128). Using (129) to write the delta function on k_2 as a delta function on $\cos\theta$, the θ integration in (132) can be done. Since the integrand is symmetric in the summation index n and the $n = 0$ term vanishes, we find for the amplitude of the pressure fluctuations

$$\frac{\langle p^2(x_2;\alpha)\rangle}{\rho^2} = \frac{4N}{\alpha^3}\frac{s_0^2}{\Delta}\int_0^{2\pi}d\phi\int_{2\pi/\Delta}^{\infty}dk\,\frac{E(k)}{k^3}\frac{\cos^2\phi}{f(\phi)}\sum_{n=1}^{[k\Delta/2\pi]}\left[\frac{2\pi n}{k\Delta}\right]^2\left[1-\left[\frac{2\pi n}{k\Delta}\right]^2\right]\frac{1}{g(\theta_n,\phi)}$$

$$\times\,[\Gamma_1^2(\mathbf{k}',x_2) + \Gamma_2^2(\mathbf{k}',x_2)]\,, \tag{134}$$

where

$$\sin^2\theta_n = 1-\left[\frac{2\pi n}{k\Delta}\right]^2. \tag{135}$$

Equation (134) was integrated numerically using the DIA spectrum for $\alpha = 4{,}8$ and the results for Reynolds numbers of 12300, 30800, and 50000 are displayed in Figs. (13) and (14). Relative to the $\alpha = 1$ case, the pressure at the wall is reduced by a factor of approximately $1/\alpha$, i.e., with the pressure in units of ρU_τ^2,

$$p_{wall}(\alpha) \approx \frac{1}{\alpha}\,p_{wall}(\alpha=1)\,. \tag{136}$$

The pressures at mid–channel have undergone relatively small changes relative to the isotropic ($\alpha = 1$) calculation, i.e.,

$$p_{midch}(\alpha) \approx p_{midch}(\alpha=1) \, . \tag{137}$$

It seems clear that the inclusion of the effects of anisotropy in the calculation of the amplitude of the pressure fluctuations has greatly improved our predictions of the wall pressures.

c) Fraction of Scattered Power, P

We have also applied the above procedure for the modeling of the effects of anisotropy on the attenuation of a laser beam propagating through a turbulent channel flow. With the fraction of scattered power defined by (103) and (104), we integrated (104) over the physical variables, using the DIA spectrum and the expressions from above for the anisotropic pressure function. The scattered fraction P was calculated for channel widths Δ = 2, 3, and 5 mm at a variety of Mach numbers and the results are presented in Table VI and displayed in Fig. (15) along with the experimental results[37] at these values of Δ. The errors on the experimental results are roughly ±35%. The Mach number M_b used in Fig. (15) is the Mach number based on the bulk velocity, U_m. Using the first of (29) and the second of (30), we find that M_b is related to the Mach number M (based on the midchannel velocity U_0) by

$$M_b = M \left[1 - \frac{2.53}{9.268 \, R_{exp}^{0.089}} \right] . \tag{138}$$

It was found that the model fit the data very well with $\alpha = 6$ for $\Delta = 2$ mm, $\alpha = 4$ for Δ

= 3 mm, and $\alpha = 5$ for $\Delta = 5$ mm. These are the best fit results; however, within the errors, the data can be adequately fit for $\alpha = 5$. It was found that over the range $1 \leq \alpha \leq 10$, the scattered fraction P decreases with α roughly as

$$P(\alpha) \approx P(\alpha=1)e^{-(\alpha-1)/3} . \tag{139}$$

XII. SUMMARY AND CONCLUSIONS

By inspecting our results, it can be concluded that the GISS model and the DIA provide a reasonable first description of both turbulent bulk properties as well as properties that depend strongly on the large eddy part of the energy spectrum. Several reservations and directions for future work have to be discussed.

First, the DIA yields larger values for the wall pressure and fraction of scattered power than the GISS model. This behavior can be understood by inspecting, for example, Eq. (94) which shows that the largest contribution to $\Pi(\mathbf{k})$, and ultimately to P, comes from the small k region of the turbulent energy spectrum. As one can see from Fig. 5, at low wave numbers the GISS E(k) is "skinnier" than the one derived from DIA. This means that the contribution to $\Pi(\mathbf{k})$ from the GISS model begins only at, say, kD =15, while in the DIA case the contribution begins earlier, i.e., at smaller wavenumbers. (The DIA energy spectrum extends in principle to zero wavenumber, but the integration over the angles in Eq. 92 and the presence of the delta function in Eq. 94 force the first contribution to begin at $kD = \pi$.) The physical reason behind the different low k behavior of the two spectral functions is known. The DIA model includes backscatter, i.e., energy transferred from the high k region into the low k region. By contrast, the present version of the GISS model is a cascade model with no backscatter as yet. While this limitation had been recognized in earlier work,[14,19] it had never been evidenced as clearly as in the present

case, since our earlier works were primarily concerned with the description of turbulent bulk properties which are relatively insensitive to the small k behavior of the turbulent spectral function. Work to include backscatter in the GISS model is now in progress.

A second comment concerns the role of shear and the way it has been treated in the present paper. The work of Tchen[11] has demonstrated that the shear may play two roles, as a source of energy and as a force interacting with the eddies. While the first role is always present, the second becomes important only when the shear s is of the same order or larger than the eddy vorticity in a given wavenumber region. When this is the case, a resonance takes place which may be more important than the effects of non–linear transfer among the eddies, represented by the function T(k) in Eq. (2). When this type of resonance dominates over the other forces, Tchen's model predicts the existence of a k^{-1} region in the energy spectrum which has indeed been observed. Our model does not include this resonance effect, the shear playing in fact only one role, that of a source of energy drained from the mean flow. This can clearly be seen by inspecting Eqs. (2)–(3) where the presence of shear is confined entirely to the left hand side of the equation in the rate $n_s(k)$, whose form is given by Eq. (53). It is clearly seen that of the two terms, the first, Im(Q), is proportional to the shear, $U'(y)$, while the other term represents a sink due to viscosity.

A third comment refers to the choice of the growth rate. Orszag and Patera[35] (hereafter referred to as O–P) have pointed out that the adoption of a Poiseuille flow with a central line velocity U_0 (used to construct a Reynolds number which is then identified with the experimental value), leads to a growth rate that, being viscid in nature is naturally rather slow. In fact, the fastest instability occurs at around R=48000 and its maximum value (n_s/n_*) is only 0.0076. O–P discovered that there is a secondary, three dimensional instability that, catalyzed by the previous one, grows much faster than the original instability. The O–P discovery is an important one in many respects, but

particularly when one is concerned with the problem of the transition between laminarity and turbulence, since it explains in a natural way (i.e. without free parameters) experimentally important features that would otherwise be left unexplained,[36] the most important being the well known fact that linear analysis predicts a breakdown of laminarity at R_{exp}=5772 while the experimental value is close to R_{exp}~2500. It is much less clear, however, whether the O–P secondary instability and its corresponding growth rate is directly relevant to our problem, where we have to deal with one important aspect that does not enter into the O–P problematics, namely the fact alluded to previously, that in the construction of n_s for our problem we must somehow take into account the renormalizing effect of the presence of turbulence itself. The physical model that we have proposed in Section IV can be viewed as a way to renormalize the central line velocity due to the presence of turbulence. Another important aspect of the physical effect brought about by the existence of the O–P secondary waves is displayed in Figure 4 of the O–P paper, where it is shown that the growth rate versus Reynolds number curve reaches a maximum and then saturates rather than decreasing as it would in the case of a viscid instability. Two facts must be noticed. The maximum value of the O–P growth rate is around 0.1, which is the same as we have obtained using our renormalization (see Fig. 3). Secondly, as it is also clear from Fig. 3, in the region of Reynolds numbers of interest in this problem, the growth rates have similar maximum values, thus indicating that we are dealing with a region where the stabilizing effect of decreasing viscosity has not yet taken place. The numerical similarity between our results and those of O–P constitutes, however, no guarantee that the O–P mechanism (to generate a growth rate) and our method are physically equivalent. Since our results for the bulk properties are in general smaller than the experimental values, it is conceivable that the use of an O–P growth rate together with a renormalization of some of the physical parameters, could yield better results. Since, however, the solution of the O–P equation, which in turn requires the exact solution of the Navier–Stokes equations for the 2–dimensional instability, would be a

non–trivial addition to our problem, we decided in this first paper to adopt the physical argument discussed above. The use of the O–P growth rate mechanism is presently under investigation.

In conclusion, while the use of theoretical models of turbulence has reproduced several properties of turbulent channel flow, limitations have also appeared. Work to include backscatter in the GISS model and to understand the role of the secondary instability is now in progress.

ACKNOWLEDGEMENT

The authors would like to thank H. Robey and S. Sutton for many helpful discussions and D. Henningson for providing the use of his Orr–Sommerfeld code.

REFERENCES

[1] J. Laufer, Nat. Adv. Comm. Aeron., Rep. No. 1053 (1951).

[2] G. Comte–Bellot, Ph.D. thesis, University of Grenoble, France,(1963).

[3] J. A. Clark, Trans. A.S.M.E. D, J. Basic Engin. **90**, 455 (1968).

[4] A. K. M. Hussain and W. C. Reynolds, Trans. A.S.M.E. I, J. Fluids Engin. **97**, 568 (1975).

[5] W. W. Willmarth, Ann. Rev. of Fluid Mech. **7**, 13, (1975).

[6] A. V. Johansson and P. H. Alfredsson, J. Fluid Mech. **122**, 295 (1982).

[7] J. Kim, P. Moin, and R. Moser, J. Fluid Mech. **177**, 133 (1987).

[8] P. Moin and J. Kim, J. Fluid Mech. **118**, 341 (1982).

[9] K. Hanjalic and B. E. Lauder, J. Fluid Mech. **52**, 609 (1972).

[10] J. O. Hinze, *Turbulence* (McGraw–Hill, New York, 1975).

[11] C. M. Tchen, J. Res. Nat. Bur. Standards **50**, 51 (1953).

[12] D. C. Leslie, *Developments in the Theory of Turbulence* (Clarendon, Oxford, 1973).

[13] R. H. Kraichnan, Phys. Fluids **7**, 1048 (1964).

[14] V. M. Canuto, I. Goldman and J. Chasnov, Phys. Fluids **30**, 3391 (1987).

[15] G. K. Batchelor, *The Theory of Homogeneous Turbulence* (Cambridge U. P., Cambridge, 1953).

[16] R. H. Kraichnan, *Phys. Fluids*, **7**, 1030 (1964).

[17] M. Lesieur, *Turbulence in Fluids*, (M. Nighoff Publ., 1987).

[18] P. C. Martin, E. D. Siggia and H. A. Rose, Phys. Rev. A **8**, 423 (1973).

[19] G. J. Hartke, V. M. Canuto and W. P. Dannevick, Phys. Fluids **31**, 256 (1988).

[20] J. L. Synge, Semi–Centenn. Publ. Am. Math. Soc. **2**, 227 (1938).

[21] C. C. Lin, *The Theory of Hydrodynamic Stability* (Cambridge U. P., Cambridge, 1955).

[22] D. Koppel, J. of Math. Phys. **5**, 963 (1964).

[23]P. G. Drazin and W. H. Reid, *Hydrodynamic Stability* (Cambridge U. P., Cambridge, 1982)

[24]A. A. Townsend, *The Structure of Turbulent Shear Flow* (Cambridge U. P., Cambridge, 1976).

[25]A. S. Monin and A. M. Yaglom, *Statistical Fluid Mechanics* (M.I.T. P., Cambridge, 1975).

[26]W. C. Reynolds and W. G. Tiederman, J. Fluid Mech. **27**, 253 (1967).

[27]G. R. Ierley and W. V. R. Malkus, J. Fluid Mech. **187**, 435 (1988).

[28]R. H. Kraichnan, J. of the Acoust. Soc. Am. **28**, 64 (1956).

[29]R. H. Kraichnan, J. of the Acoust. Soc. Am. **28**, 378 (1956).

[30]G. K. Batchelor, Proc. Cambridge Phil. Soc. **47**, 359 (1951).

[31]W. K. Blake, J. Fluid Mech., **44**, 637 (1970).

[32]R. A. Handler, R. J. Hansen, L. Sakell, S. A. Orszag, and E. Bullister, Phys. Fluids, **27**, 579 (1984).

[33]C. B. Hogge, R. R. Butts and M. Burlakoff, Applied Optics **13**, 1065 (1974).

[34]V. I. Tatarskii, *Wave Propagation in a Turbulent Medium* (McGraw–Hill, New York, 1961).

[35]S. A. Orszag and A. T. Patera, J. Fluid Mech. **128**, 347 (1983).

[36]J. T. Stuart, in *Transition and Turbulence*, ed. by R. E. Meyer (Acad. Press), 77, (1981).

[37]G. F. Albrecht and S. Sutton, LLNL Report (October 1987).

Table I

R_{exp}	R_T	R_m	r_1	r_2
10^4	500	8735	12.55	9.54
2×10^4	925	17659	21.00	16.15
3×10^4	1331	26633	29.00	22.20

Table II

The growth rate $n_s(k)$ vs. k from a solution of the Orr–Sommerfeld equation for four values of the Reynolds number, R_{exp}. (The unit n_* is given by Eq. 52).

$R_{exp} = 12{,}300$		$R_{exp} = 28{,}600$		$R_{exp} = 30{,}800$		$R_{exp} = 50{,}000$	
kD	$10n_s/n_*$	kD	$10n_s/n_*$	kD	$10n_s/n_*$	kD	$10n_s/n_*$
8.631	0.125	10.533	0.173	10.700	0.168	12.74	0.410
9.081	0.291	11.265	0.414	11.256	0.356	14.51	0.838
9.588	0.447	12.113	0.643	11.886	0.537	16.57	1.19
10.144	0.589	13.053	0.849	12.578	0.709	18.85	1.41
10.739	0.713	14.068	1.025	13.323	0.867	21.33	1.42
11.369	0.813	15.147	1.158	14.112	1.006	24.0	1.08
12.031	0.886	16.285	1.234	14.940	1.123	27.1	0.117
12.721	0.927	17.479	1.254	15.804	1.212		
13.441	0.930	18.732	1.183	16.702	1.268		
14.189	0.889	20.053	1.003	7.634	1.283		
14.972	0.796			18.599	1.251		
15.794	0.645			19.603	1.160		
				20.650	0.998		

Table III

k_y as a function of $k_\perp$ computed from Eq. (58) for three values of the Reynolds number.

$R_{exp} = 12{,}300$		$R_{exp} = 30{,}800$		$R_{exp} = 50{,}000$	
$k_\perp D$	$k_y D$	$k_\perp D$	$k_y D$	$k_\perp D$	$k_y D$
0.453	8.62	0.425	13.3	0.32	12.7
0.48	9.07	0.485	15.8	0.36	14.5
0.507	9.58	0.505	16.7	0.40	16.6
0.533	10.1	0.525	17.6	0.44	18.8
0.56	10.7	0.545	18.6	0.48	21.3
0.587	11.4	0.565	19.6	0.52	24.0
0.613	12.0	0.585	20.6	0.56	27.1
0.64	12.7	0.605	21.7		
		0.625	22.9		

Table IV

	$R_{exp} = 12{,}300$			$R_{exp} = 30{,}800$			$R_{exp} = 50{,}000$
	GISS	DIA	EXP	GISS	DIA	EXP	GISS
$10^3\langle u^2\rangle$	0.920	1.14		1.16	1.21		1.25
$10^2\langle u_x^2\rangle^{\frac{1}{2}}$	1.75	1.95	3.6	1.96	2.01	3.0	2.00
$10^4\nu_t$	6.30			5.04			4.30
$10^5\epsilon$	4.70	5.43		7.12	7.53	3.62	9.08
λ_x	0.192	0.092	0.11	0.15	0.051	0.095	0.141
Λ_x	0.857	1.05		0.60	0.80	0.63	0.49
$10^3\ell_0$	10.3	9.97		4.70			

Table V

Values of 10^2P, Eq. (102),and full channel width Δ (in mm) for different Mach and Reynolds numbers.

$R_{exp} = 12300$

M	Δ	GISS	DIA
0.1	5.71	6.50×10^{-4}	1.04×10^{-3}
0.114	5.00	8.49×10^{-4}	1.36×10^{-3}
0.190	3.00	2.36×10^{-3}	3.77×10^{-3}
0.2	2.86	2.59×10^{-3}	4.16×10^{-3}
0.286	2.00	5.30×10^{-3}	8.48×10^{-3}
0.3	1.90	5.82×10^{-3}	9.35×10^{-3}
0.4	1.43	1.04×10^{-2}	1.66×10^{-3}
0.5	1.14	1.62×10^{-2}	2.59×10^{-2}
0.6	0.952	2.33×10^{-2}	3.72×10^{-2}
0.7	0.816	3.23×10^{-2}	5.07×10^{-2}

$$R_{exp} = 30800$$

M	Δ	GISS	DIA
0.1	14.3	9.04×10^{-3}	1.81×10^{-2}
0.2	7.15	3.56×10^{-3}	7.23×10^{-2}
0.286	5.00	7.38×10^{-2}	0.148
0.3	4.77	8.08×10^{-2}	0.162
0.4	3.58	0.144	0.289
0.477	3.00	0.205	0.410
0.5	2.86	0.225	0.450
0.6	2.38	0.324	0.649
0.7	2.04	0.438	0.883
0.715	2.00	0.459	0.920

$$R_{exp} = 50000$$

M	Δ	GISS	DIA
0.1	23.2	3.33×10^{-2}	4.30×10^{-2}
0.2	11.6	0.133	0.183
0.3	7.74	0.297	0.413
0.4	5.81	0.530	0.734
0.465	5.00	0.714	0.987
0.5	4.65	0.827	1.14
0.6	3.87	1.19	1.64
0.7	3.32	1.59	2.23
0.774	3.00	1.97	2.71
1.16	2.00	4.35	5.99

Gas properties: $\nu = 8.6\times10^{-2}$ cm^2 sec^{-1}, $\rho = 2.07\times10^{-3}$ gm cm^{-3}, p = 2 atm, $\mu = 28$ gm mole^{-1}.

Optical properties: wavelength $\lambda = 0.53$ microns, refractive index $n_r = 1.53$.

Table VI

Values of 10^2P for full channel width

Δ = 2, 3, and 5 mm.

Δ = 2 mm

R_{exp}	M	M_b	10^2 P		
			$\alpha = 1$	$\alpha = 4$	$\alpha = 8$
12,300	0.286	0.252	8.48×10^{-3}	2.80×10^{-3}	7.86×10^{-4}
30,800	0.715	0.638	0.920	0.315	8.89×10^{-2}
50,000	1.16	1.04	5.99	2.25	0.662

Δ = 3 mm

R_{exp}	M	M_b	10^2 P		
			$\alpha = 1$	$\alpha = 4$	$\alpha = 8$
12,300	0.190	0.168	3.77×10^{-3}	1.24×10^{-3}	3.49×10^{-4}
30,800	0.477	0.425	0.410	0.140	3.95×10^{-2}
50,000	0.774	0.694	2.71	1.01	0.295

Δ = 5 mm

R_{exp}	M	M_b	10^2 P		
			$\alpha = 1$	$\alpha = 4$	$\alpha = 8$
12,300	0.114	0.101	1.36×10^{-3}	4.47×10^{-4}	1.26×10^{-4}
30,800	0.286	0.255	0.148	5.05×10^{-2}	1.42×10^{-2}
50,000	0.465	0.416	0.987	0.363	0.106

FIGURE CAPTIONS

Figure 1. The expected general shape of the growth rate $n_s(k)$ vs. k. At large wavenumbers, $n_s(k)$ tends to $-\nu k^2$.

Figure 2. The growth rate $n_s(k)$ vs. k in units of n_*, Eq. (52), as solution of the Orr–Sommerfeld equation for R_{exp}= 12300, 30800, and 50000.

Figure 3. The GISS turbulent energy spectral function F(k), in units of F_*, Eq. (59), vs.k for R_{exp}= 12300, 30800, and 50000.

Figure 4. A comparison of the GISS and DIA spectral functions for R_{exp}= 30800. (Same units as in Fig. 4)

Figure 5. The energy $\epsilon(k)$ per unit mass and time, Eq. (7), in units of ϵ_*, Eq. (60), for several values of R_{exp}. As one may note, the function saturates very rapidly, thus becoming independent of the wavenumber k.

Figure 6. The turbulent viscosity $\nu_t(k)$ vs. k, Eq. (8), in units of ν_*, Eq. (61), for several values of R_{exp}.

Figure 7. Comparison of the theoretical one–dimensional spectral function, Eq. (63), vs. k_1 (full line), with the one measured by Hussain and Reynolds[4] for R_{exp}= 28600, U_0= 1350 cm sec^{-1} and D = 3.18 cm.

Figure 8. Comparison of the theoretical one–dimensional spectral function defined by Eq. (64) with the one measured by Laufer[1], corresponding to R_{exp}= 30800. U_0=728 cm sec^{-1} and D = 6.35 cm.

Figure 9. The value of the fluctuating pressure, in units of ρU_τ^2 computed from Eq. (93), as a function of distance across the channel of width Δ=2D. The results are computed using the GISS model.

Figure 10. Same as Figure 10, but computed using the DIA model.

Figure 11. The quantity 10^2P, Eq (102), versus M^4 for three values of the channel width Δ = 2, 3, 5 mm.

Figure 12. Same as Fig. 8, but also for α= 4 and 8.

Figure 13. Same as Fig. (10), but for α = 4.

Figure 14. Same as Fig. (10), but for α = 8.

Figure 15. The quantity 10^2P versus the fourth power of the bulk Mach number, M_τ^4 (see text), for three values of channel width Δ = 2, 3, and 5 mm. The best fit value of α is shown. The experimental data are represented as ▽ for the 5 mm results, × for the 3 mm results, and ○ for the 2 mm results.

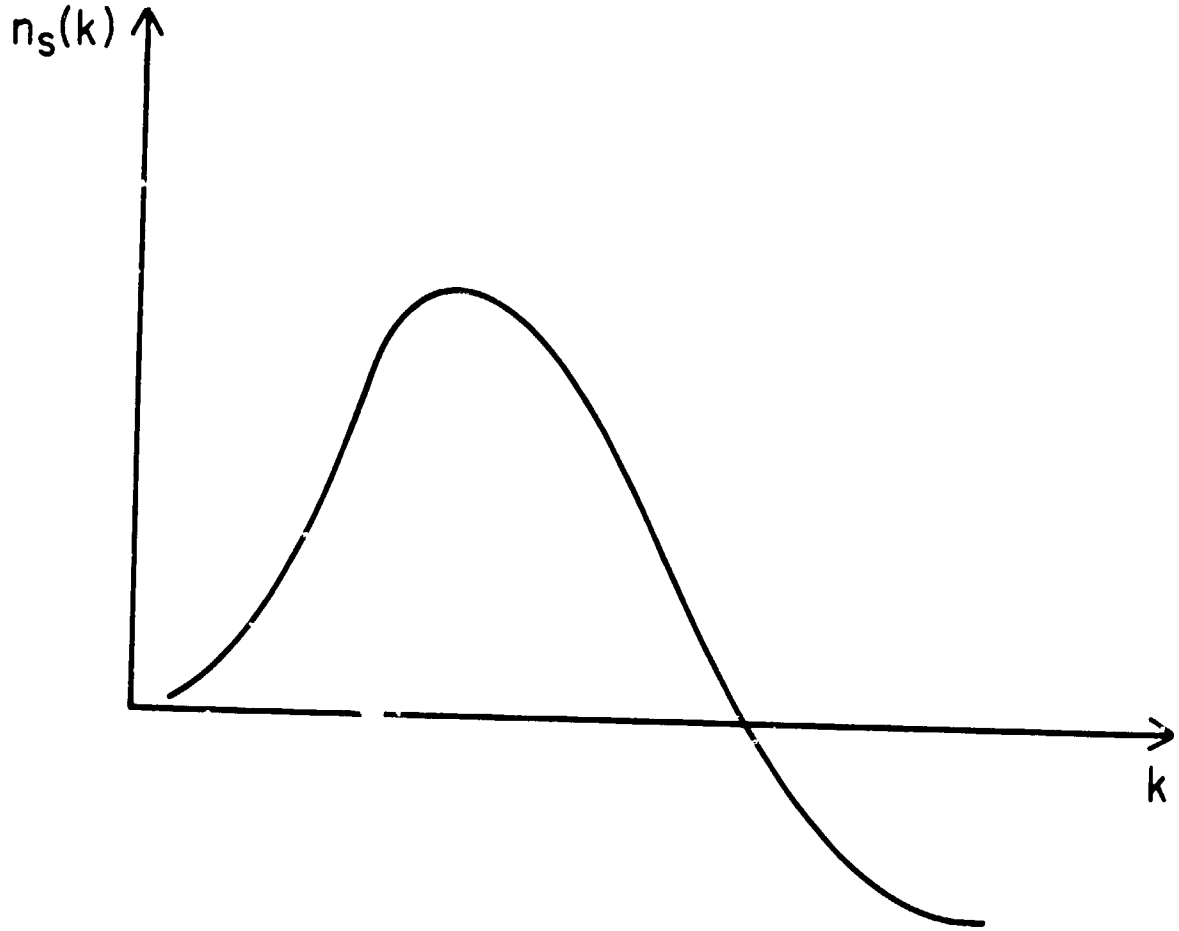

Fig. 1

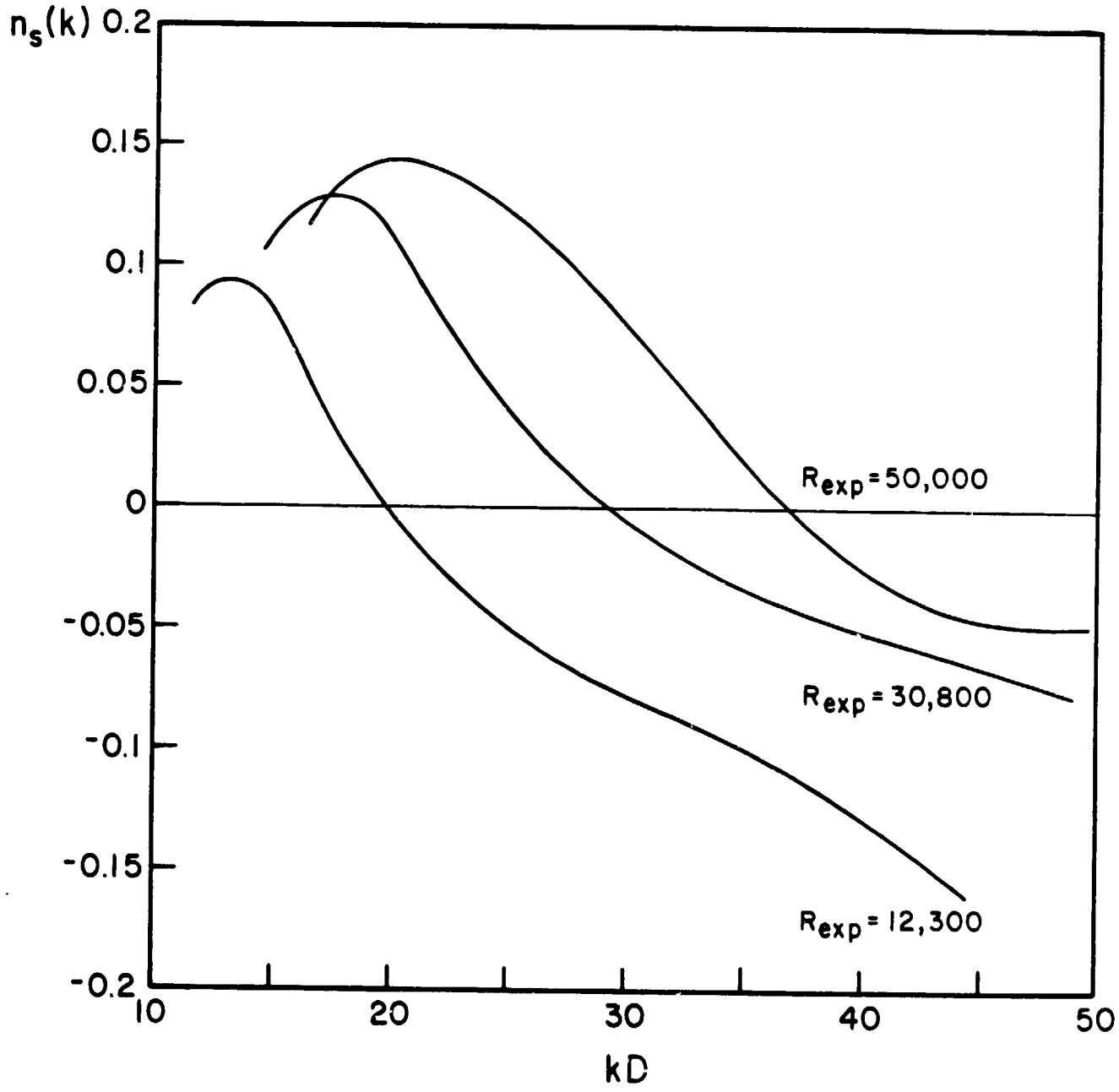
$n_s(k)$ 0.2
0.15
0.1
0.05
0
-0.05
-0.1
-0.15
-0.2
10
20
30
40
50
kD
R_{exp} = 50,000
R_{exp} = 30,800
R_{exp} = 12,300

Fig. 2

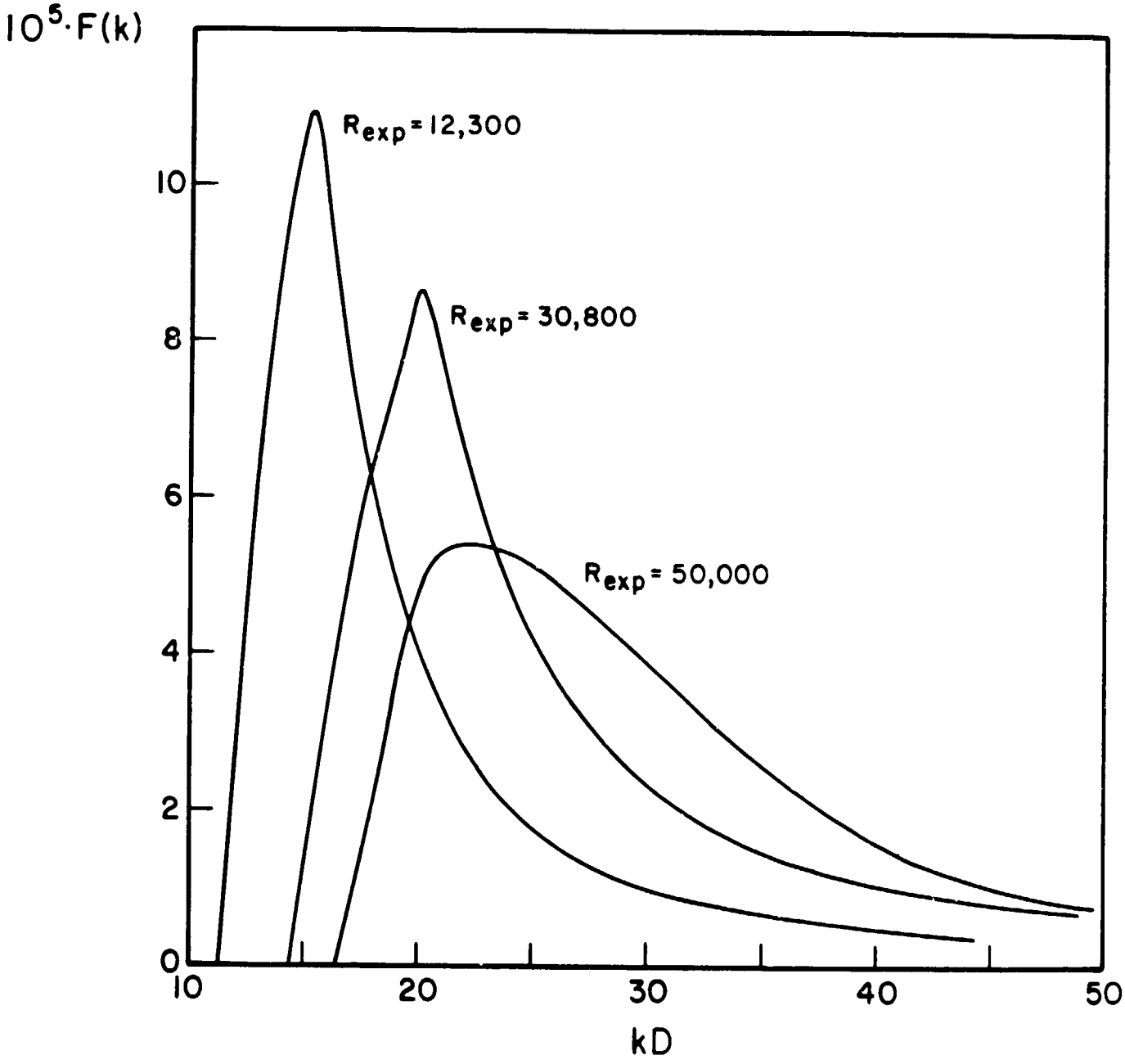
$10^5 \cdot F(k)$
R_{exp} = 12,300
R_{exp} = 30,800
R_{exp} = 50,000
0
2
4
6
8
10
10
20
30
40
50
kD

Fig. 3

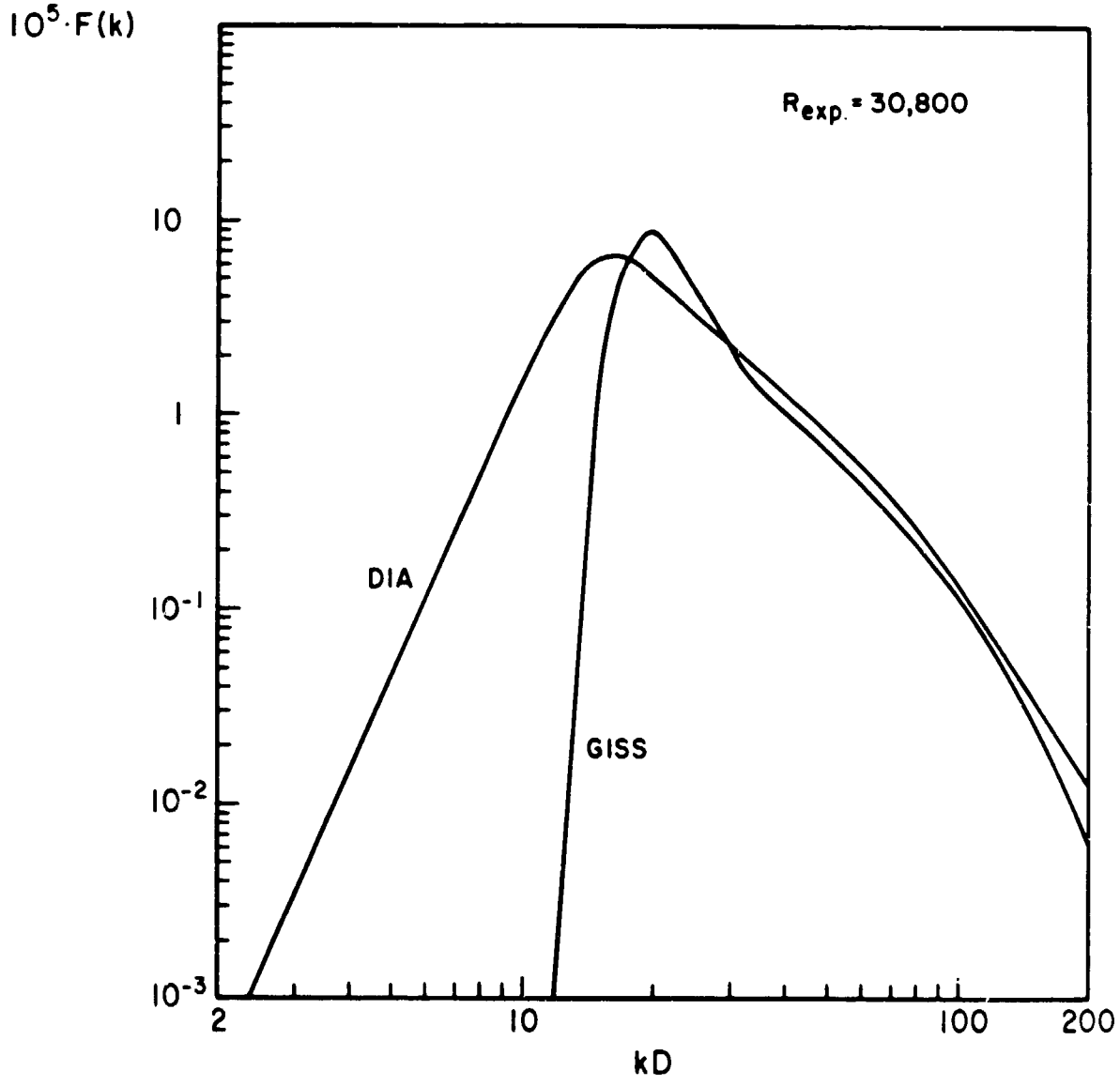

Fig. 4

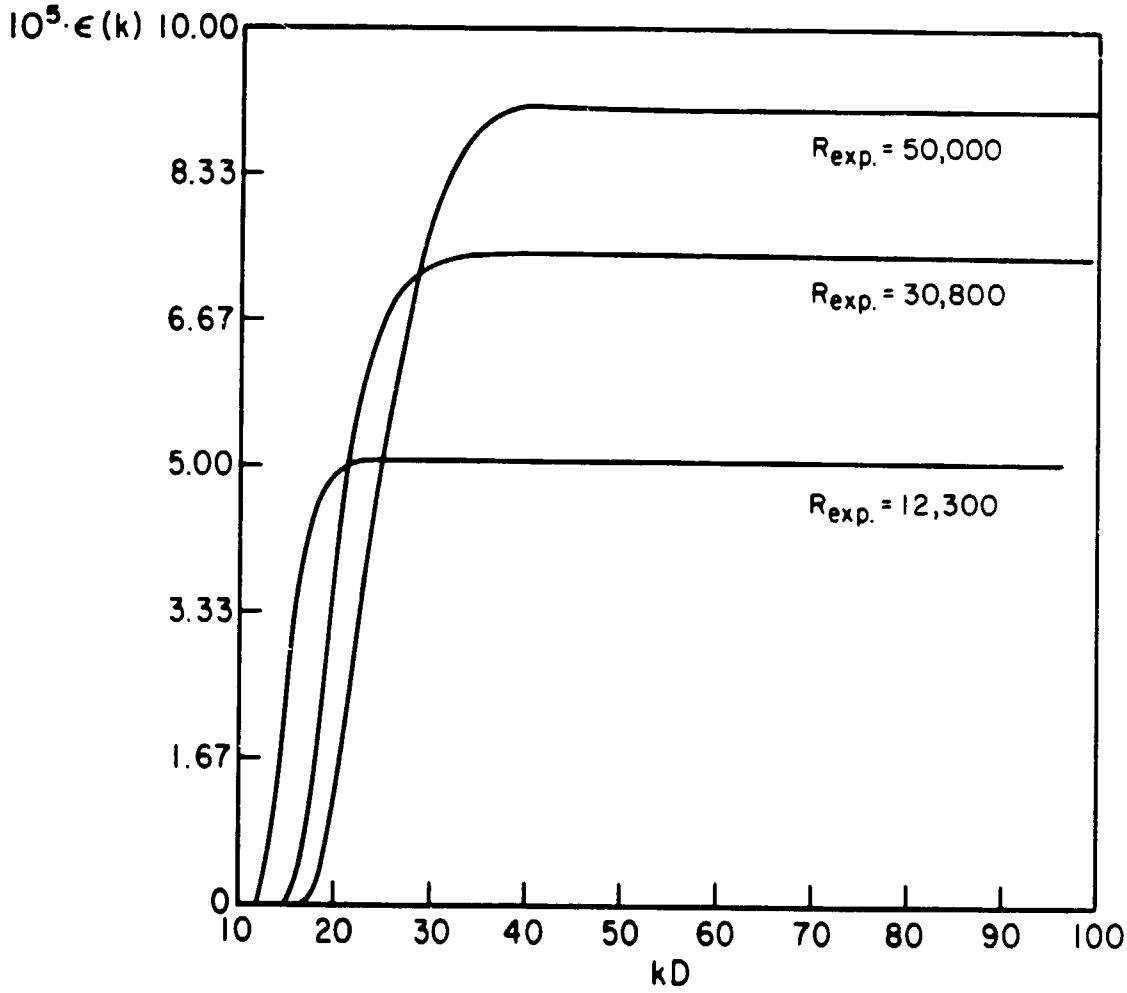
$10^5 \cdot \epsilon(k)$ 10.00
8.33
6.67
5.00
3.33
1.67
0
$R_{exp.}$ = 50,000
$R_{exp.}$ = 30,800
$R_{exp.}$ = 12,300
10
20
30
40
50
60
70
80
90
100
kD

Fig. 5

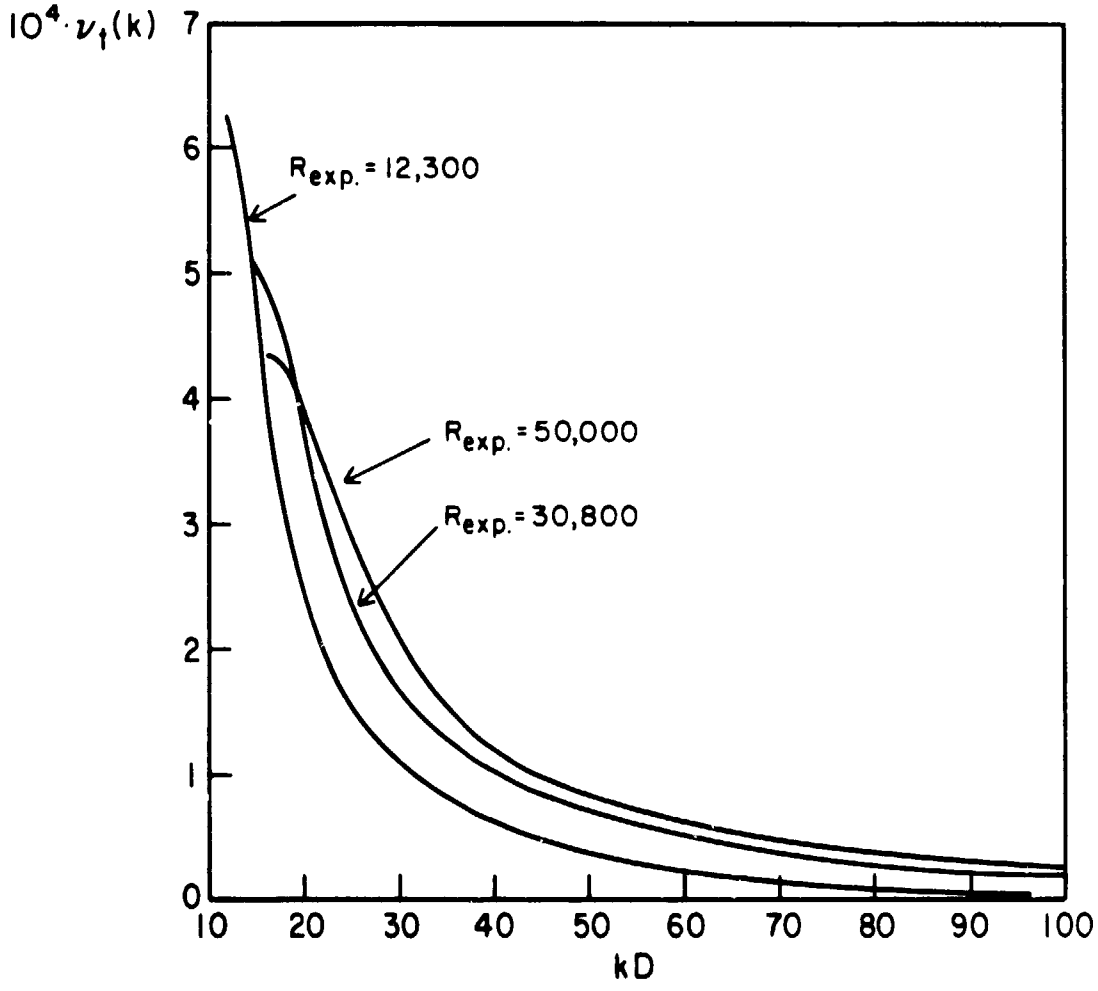
$10^4 \cdot \nu_1(k)$
7
6
5
4
3
2
1
0
$R_{exp.} = 12,300$
$R_{exp.} = 50,000$
$R_{exp.} = 30,800$
10
20
30
40
50
60
70
80
90
100
kD

Fig. 6

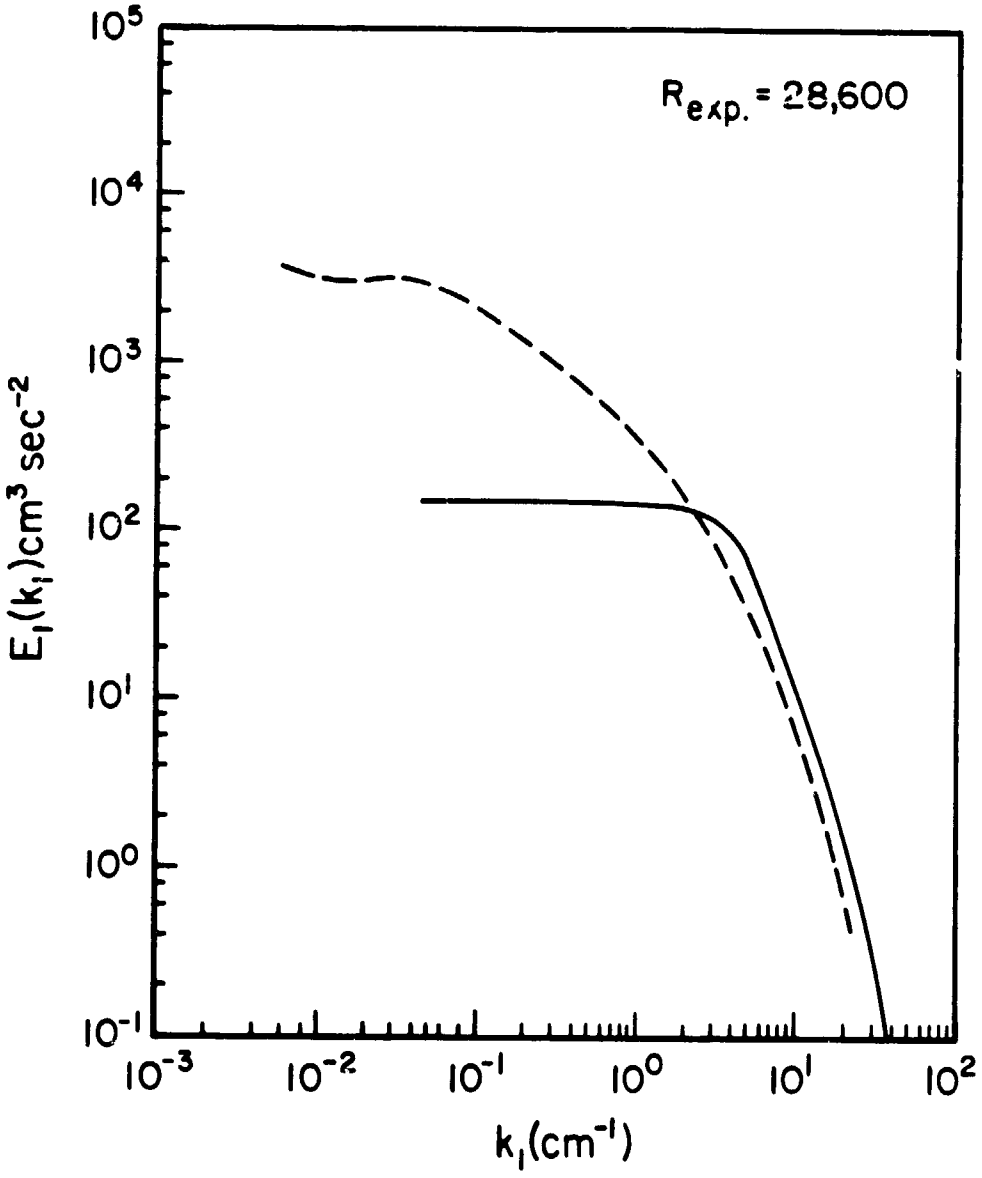
$R_{exp.} = 28{,}600$
$E_1(k_1)cm^3 sec^{-2}$
10^5
10^4
10^3
10^2
10^1
10^0
10^{-1}
10^{-3}
10^{-2}
10^{-1}
10^0
10^1
10^2
$k_1(cm^{-1})$

Fig. 7

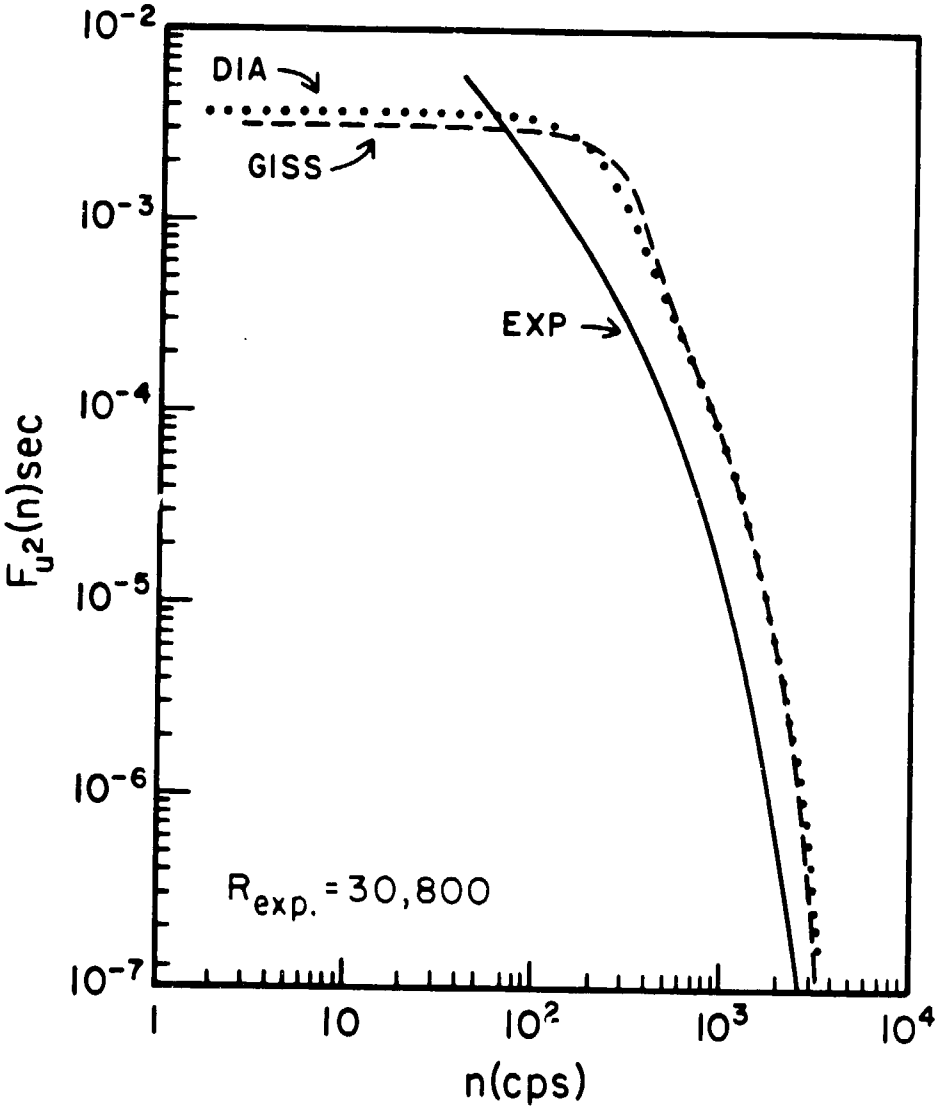
10^{-2}
10^{-3}
10^{-4}
10^{-5}
10^{-6}
10^{-7}
$F_{u2}(n)$sec
DIA
GISS
EXP
$R_{exp.} = 30,800$
1
10
10^2
10^3
10^4
n(cps)

Fig. 8

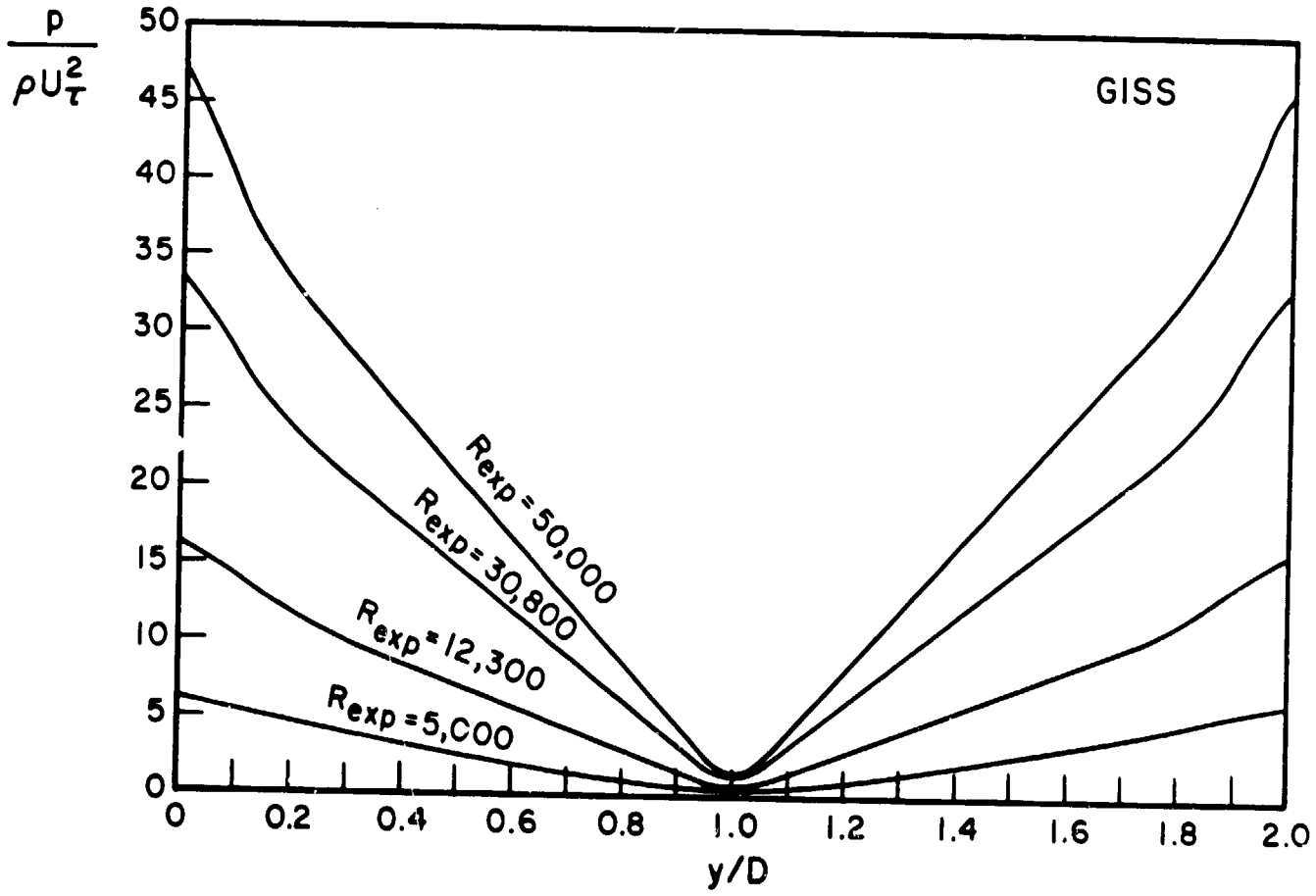
p / ρU²τ
50
45
40
35
30
25
20
15
10
5
0
GISS
Rexp = 50,000
Rexp = 30,800
Rexp = 12,300
Rexp = 5,000
0
0.2
0.4
0.6
0.8
1.0
1.2
1.4
1.6
1.8
2.0
y/D

Fig. 9

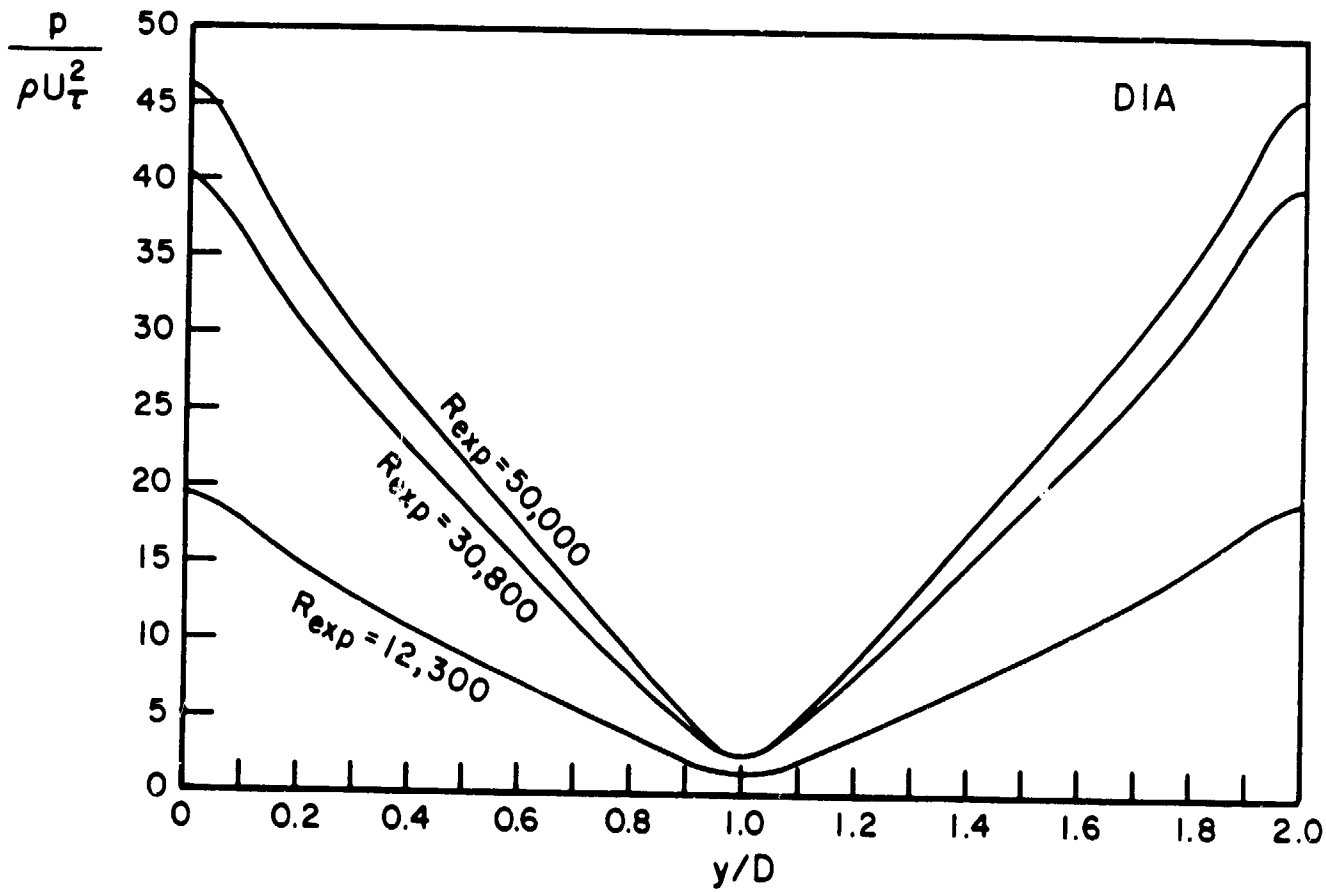
p / ρU²τ
50
45
40
35
30
25
20
15
10
5
0
DIA
Rexp = 50,000
Rexp = 30,800
Rexp = 12,300
0
0.2
0.4
0.6
0.8
1.0
1.2
1.4
1.6
1.8
2.0
y/D

Fig. 10

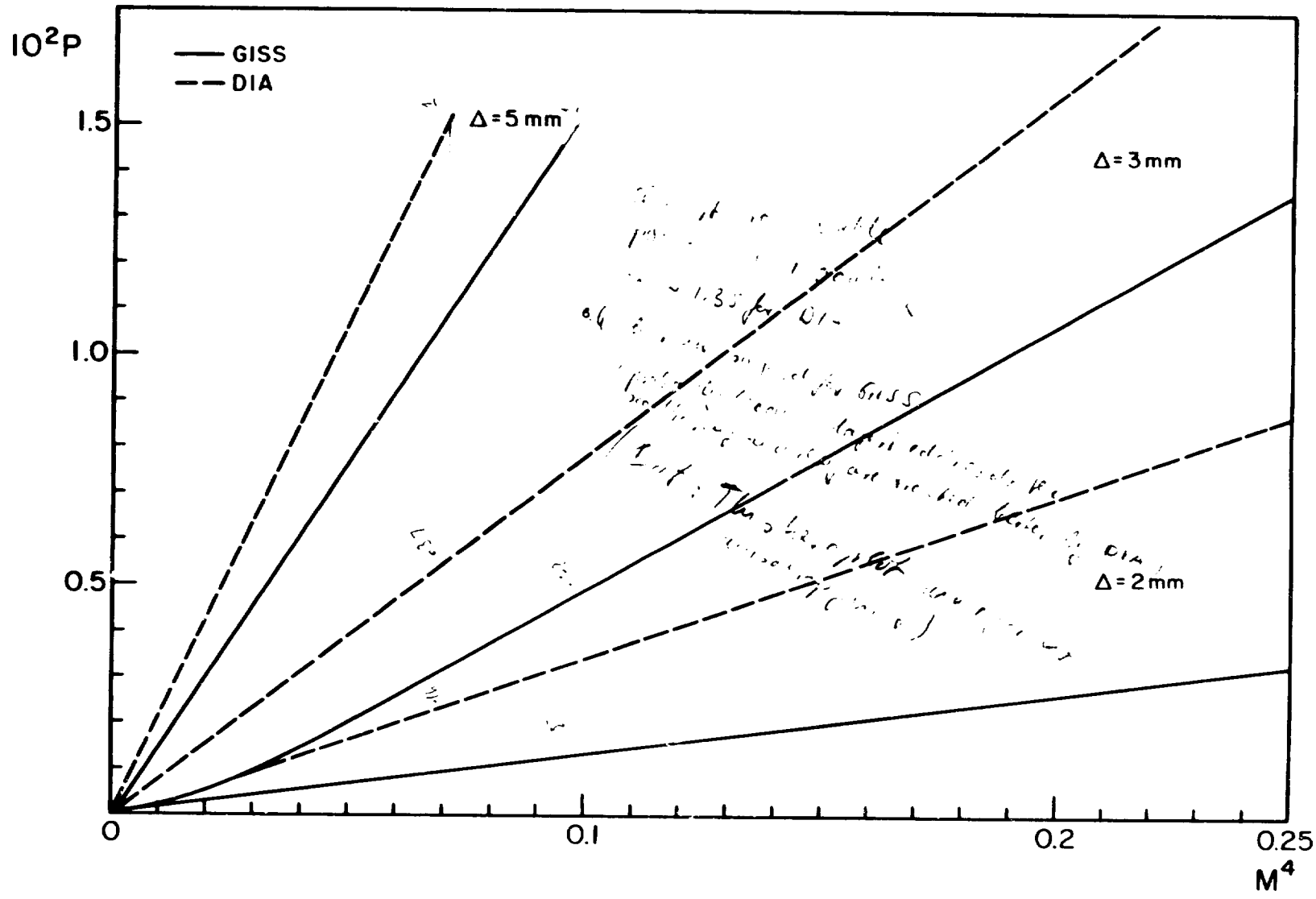

Fig. 11

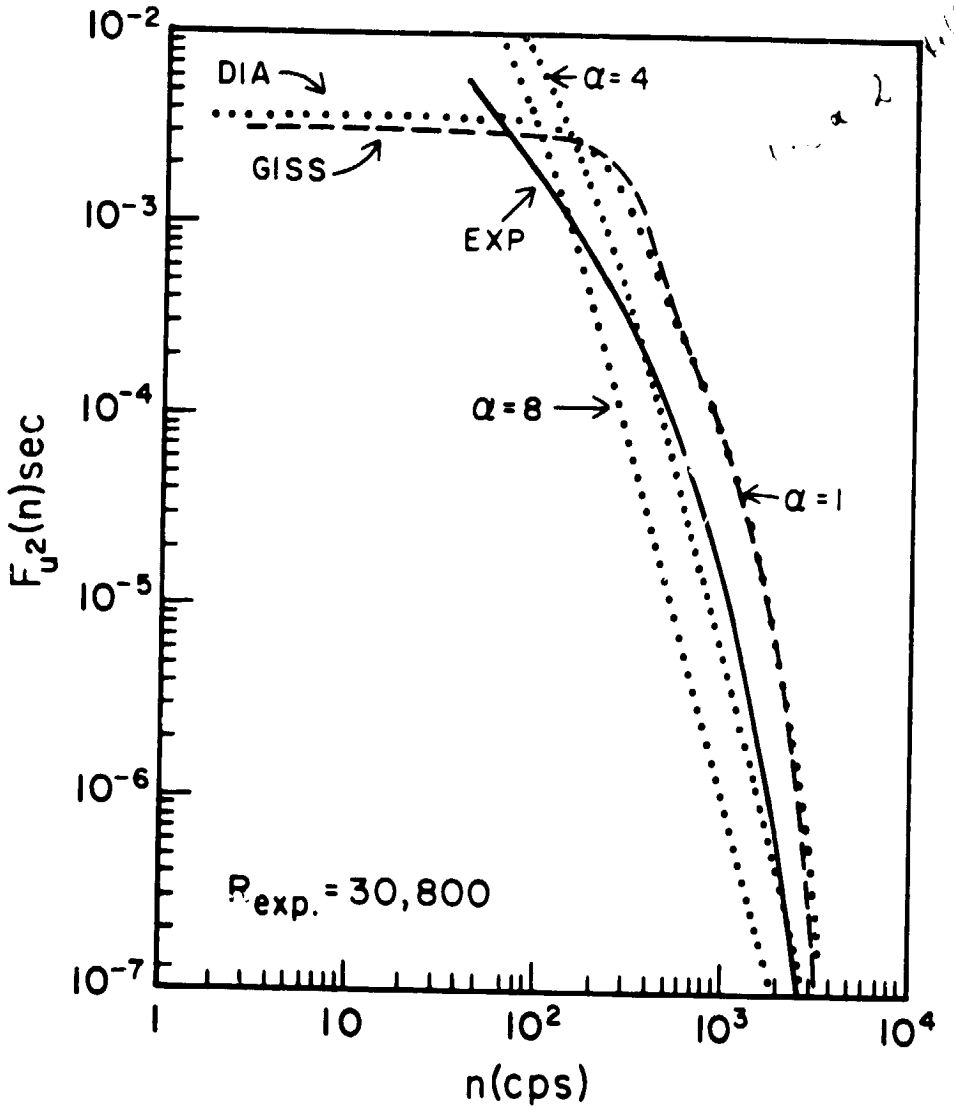
10^{-2}
10^{-3}
10^{-4}
10^{-5}
10^{-6}
10^{-7}
$F_{u2}(n)$sec
DIA
GISS
EXP
α=4
α=8
α=1
$R_{exp.}$=30,800
1
10
10^2
10^3
10^4
n(cps)

Fig. 12

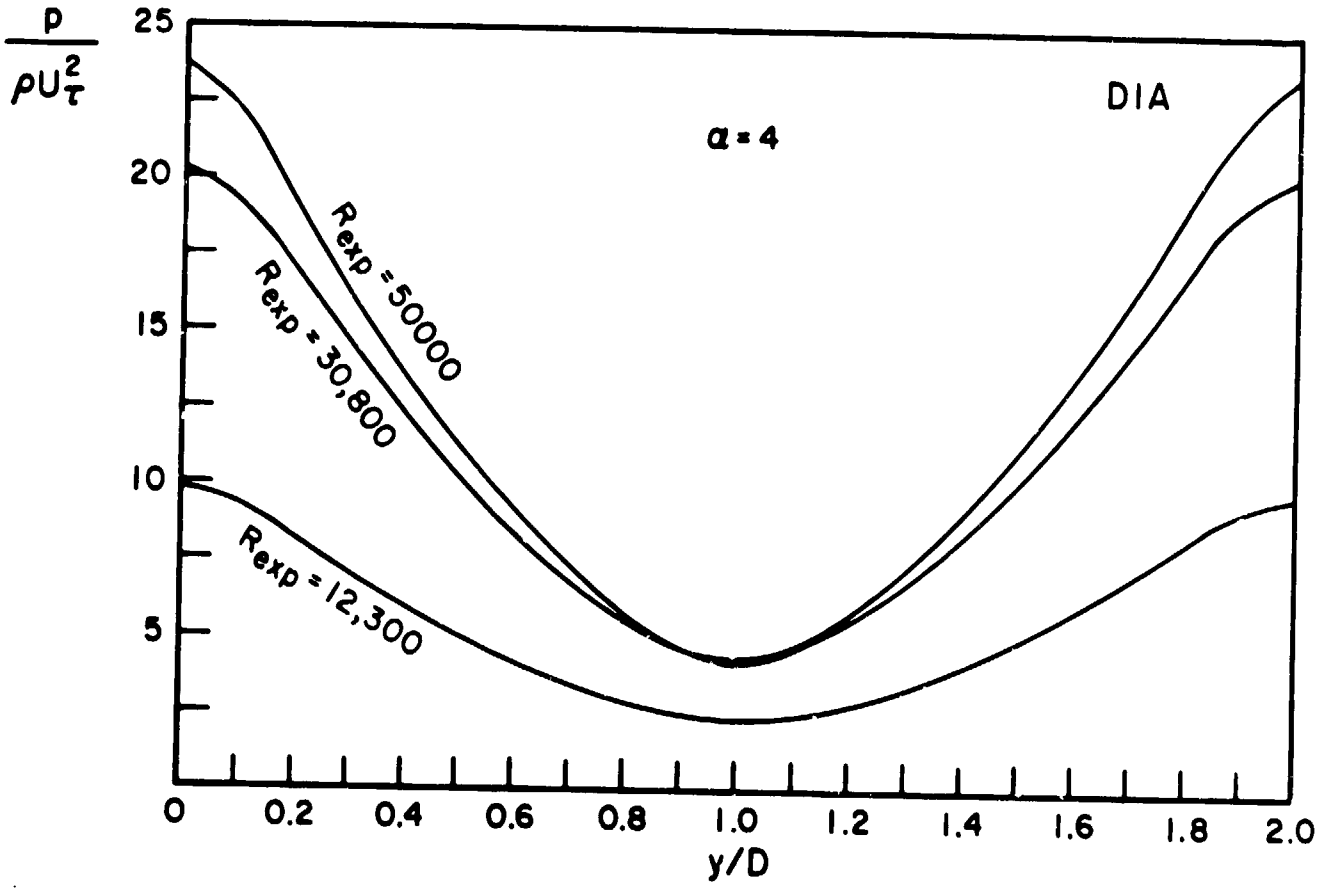
p / ρU²τ
25
20
15
10
5
DIA
α = 4
Rexp = 50000
Rexp = 30,800
Rexp = 12,300
0
0.2
0.4
0.6
0.8
1.0
1.2
1.4
1.6
1.8
2.0
y/D

Fig. 13

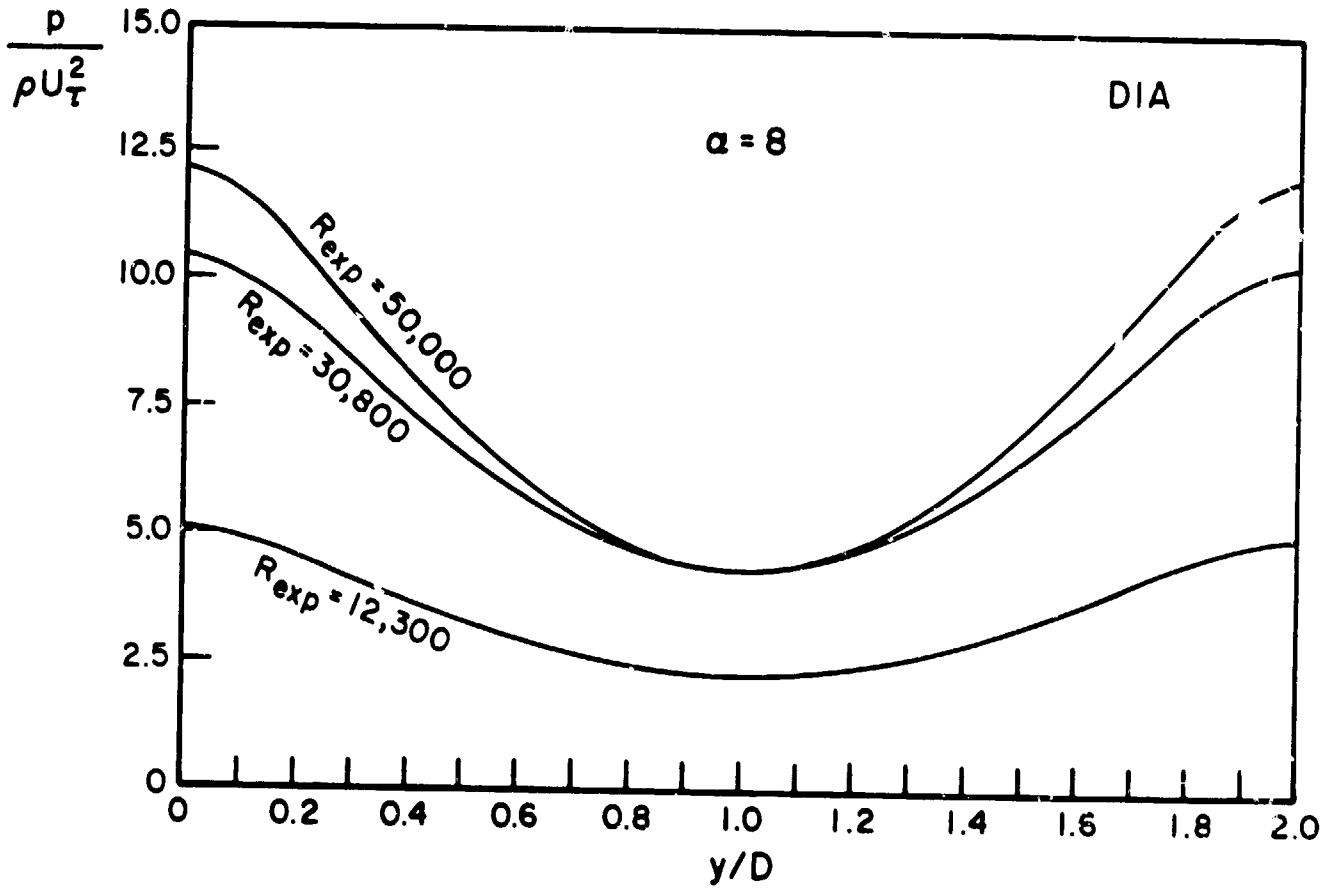
p / ρU_τ^2
15.0
12.5
10.0
7.5
5.0
2.5
0
DIA
α = 8
Rexp = 50,000
Rexp = 30,800
Rexp = 12,300
0
0.2
0.4
0.6
0.8
1.0
1.2
1.4
1.6
1.8
2.0
y/D

Fig. 14

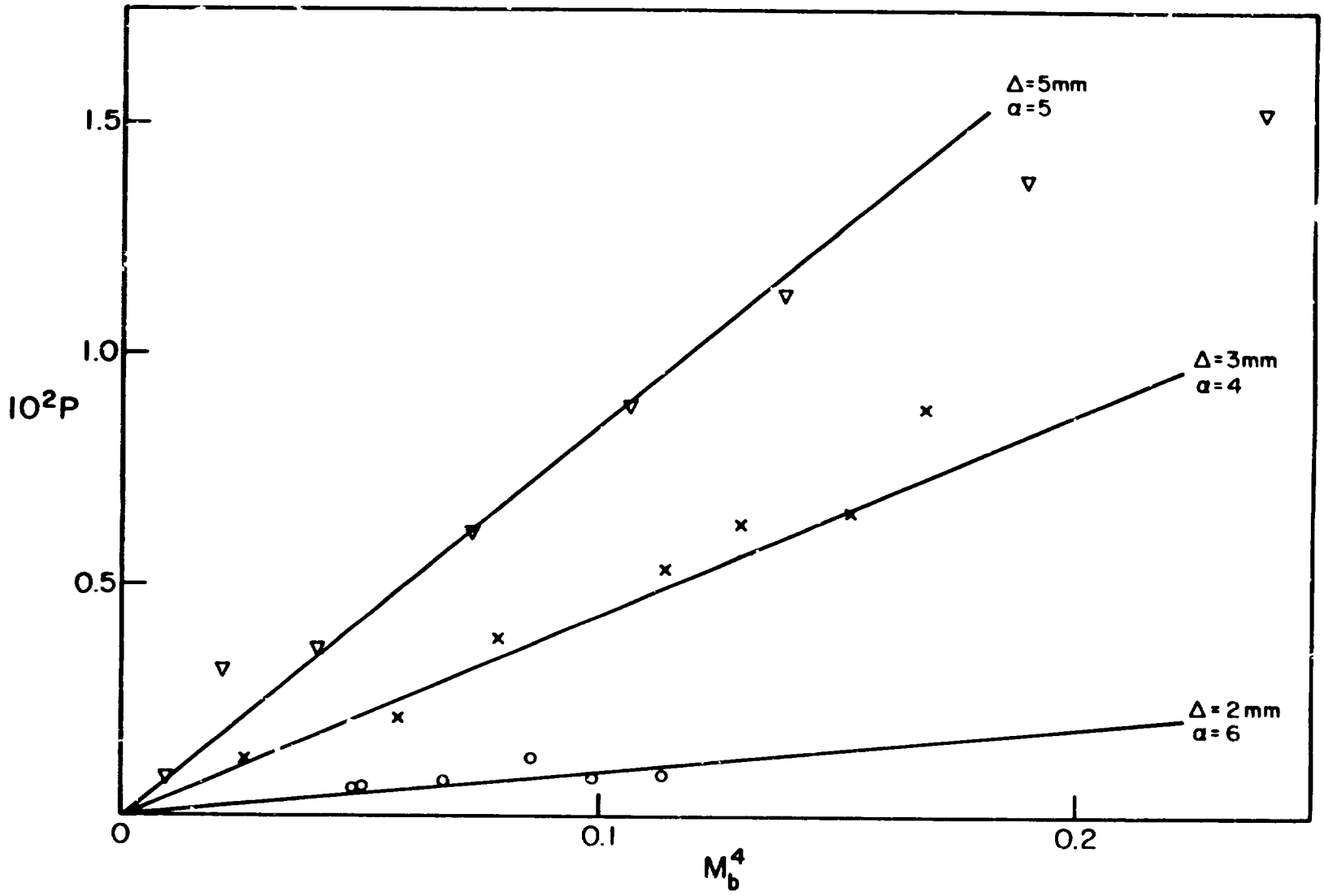

Fig. 15